# A model to predict the evolution of a gravel bed river under an imposed cyclic hydrograph and its application to the Trinity River

Enrica Viparelli,[1,2] David Gaeuman,[3] Peter Wilcock,[4] and Gary Parker[1,5]

Received 31 January 2010; revised 3 July 2010; accepted 17 November 2010; published 22 February 2011.

[1] Major changes in the morphology of the Trinity River in California, such as narrowing of the cross section and sedimentation of fine sediment in pools, occurred after the closure of a system of dams. These changes caused a dramatic reduction in the salmonid population and a resulting decline of the fishery. Gravel augmentation, regulated flood releases, and mechanical channel rehabilitation are currently being implemented to help restore the aquatic habitat of the river. The present paper describes a tool, named the Spawning Gravel Refresher, for designing and predicting the effects of gravel augmentation in gravel bed rivers. The tool assumes an imposed, cycled hydrograph. The model is calibrated and applied to the regulated reach of the Trinity River in four steps: (1) zeroing runs to reproduce conditions of mobile bed equilibrium as best can be estimated for the predam Trinity River, (2) runs to compare the predictions with the results of previous studies, (3) runs at an engineering time scale to reproduce the effects of the dams, and (4) runs to design gravel augmentation schemes. In the fourth group of runs, the combined effects of engineered flood flow releases and gravel augmentation are predicted. At an engineering time scale, the model indicates that the fraction of fine sediment in the surface layer and in the topmost part of the substrate should decrease when subjected to these two restoration measures, with a consequent improvement of the quality of the spawning gravel.

**Citation:** Viparelli, E., D. Gaeuman, P. Wilcock, and G. Parker (2011), A model to predict the evolution of a gravel bed river under an imposed cyclic hydrograph and its application to the Trinity River, *Water Resour. Res., 47*, W02533, doi:10.1029/2010WR009164.

## 1. Introduction

[2] In the early 1960s a pair of dams was built on the Trinity River, California, mainly to divert water to the basin of the Sacramento River for the development of agriculture in the Central Valley. After closure of the dams, only a very small residual discharge was released downstream, and, in addition, the coarse sediment contributed from the basin upstream of the dams was entirely captured by the reservoirs. This dramatic reduction in water discharge and coarse-sediment input caused major changes in the regulated part of the river, particularly in the stretch just below the dams, where the effects of the regulation are most strongly felt [e.g., *Wilcock et al.*, 1996]. The river lost its capacity to move gravel [e.g., *Pitlick and Wilcock*, 2001]. It narrowed [e.g., *Wilcock et al.*, 1996; *Pitlick and Wilcock*, 2001] concomitantly with vegetal encroachment [e.g., *McBain and Trush*, 1997; *Nelson et al.*, 1987], and its position within the floodplain became fixed [e.g., *Pitlick and Wilcock*, 2001]. In addition, sedimentation occurred at the confluences with major tributaries [e.g., *McBain and Trush*, 1997], and fine sediment deposited in pools [e.g., *Grant et al.*, 2003; *Lisle and Hilton*, 1992; *Nelson et al.*, 1987], therefore changing the bed topography and its grain size distribution [e.g., *Wilcock et al.*, 1996]. These changes in river morphology and flood regime have caused a sharp decline in the once-productive fishery of coho and chinook salmon and rainbow trout [e.g., *Nelson et al.*, 1987; *U.S. Fish and Wildlife Service and Hoopa Valley Tribe*, 1999]. At present, mandated annual flow releases are being implemented in conjunction with gravel augmentation and mechanical channel alterations in an attempt to improve the fluvial habitat. In particular, an annual flood hydrograph is released from the dams to reproduce some features of the unregulated flow that are necessary for the maintenance of complex bend and bed topography (i.e., armor turnover, periodic scour and fill, and bar migration) because these features promote the development and maintenance of a healthy habitat for the salmonid population [e.g., *Wilcock et al.*, 1996; *Nelson et al.*, 1987].

[3] The variations in river morphology observed in the regulated Trinity River have been observed downstream of many other dams [e.g., *Williams and Wolman*, 1984; *Harvey et al.*, 2005]. In particular, *Williams and Wolman* [1984] explained the narrowing of the cross section considering that the predam width of the channel is controlled by periodic floods capable of causing bank erosion and controlling vegetal encroachment. When these floods are eliminated or drastically reduced, low flow prevails and results

[1]Department of Civil and Environmental Engineering, University of Illinois at Urbana-Champaign, Urbana, Illinois, USA.
[2]Dipartimento di Ingegneria Idraulica ed Ambientale G. Ippolito, Università degli Studi di Napoli Federico II, Naples, Italy.
[3]Trinity River Restoration Program, Weaverville, California, USA.
[4]Department of Geography and Environmental Engineering, Johns Hopkins University, Baltimore, Maryland, USA.
[5]Department of Geology, University of Illinois at Urbana-Champaign, Urbana, Illinois, USA.


0043-1397/11/2010WR009164

in a new narrower cross section in the lowest part of the original channel. Even when high flows are generated by controlled releases from dams, the magnitude and duration as compared to predam floods may not be sufficient to maintain the predam width. The *Harvey et al.*, 2005 noted that along most of the regulated rives in the Central Valley the sediment in transport is generally finer than the channel bed sediment because the water discharges are smaller than in the unregulated rivers and also because the coarser sediment contributed from upland regions deposits in the reservoirs. Some of the consequences of these transport conditions are the reduction of channel migration rates, the development of a static armor, and the reduction in pool depths due to the sedimentation of fine sediment [e.g., *Nelson et al.*, 1987; *Pitlick and Wilcock*, 2001; *Grant et al.*, 2003].

[4] Since the 1960s, gravel augmentations have been performed downstream of several dams in Central Valley, California [*Harvey et al.*, 2005]. These projects mainly focused on improving the quality of the spawning habitat. Spawning riffles and pools were artificially reconstructed, and sometimes they were held in place with large boulders. The beneficial effects of these projects lasted for only a few years because the gravel emplaced for spawning was generally transported downstream by high flows. More recently, gravel augmentations combined with high-flow releases have been implemented not only to improve the availability and quality of the spawning gravel and of spawning and rearing habitat but also to "increase coarse sediment transport and deposition, improve channel migration and form complex bar features that will improve habitat for a variety of aquatic and terrestrial species" [*Harvey et al.*, 2005] under the regulated river regime. This second type of gravel augmentation is being implemented on the regulated reach of the Trinity River.

[5] How to predict the geomorphic consequences of a gravel augmentation project, such as its spatial and temporal effects, the variations of channel morphology, and grain size distribution of the armor layer and of the topmost part of the bed deposit, is still an open problem [e.g., *Harvey et al.*, 2005].

[6] The numerical model presented herein represents an attempt to develop a tool that helps in the design of gravel augmentation projects. In particular, it focuses on the spatial and temporal predictions of the effects that gravel augmentations may have on the grain size distribution of the armor layer and of the topmost part of the bed deposit (i.e., the layer where spawning fish deposit their eggs). These grain size distributions depend on the sediment supply and the flow regime [e.g., *Hassan et al.*, 2006], and thus, these parameters must be important considerations in designing gravel augmentations to restore habitat for the salmonid population. On the one hand, if the bed material in the bed surface becomes too coarse, spawning fish cannot move it. On the other hand, an excess of fine sediment in the substrate may result either in a reduction of permeability of the bed, causing the suffocation of salmon embryos, or the blockage of small alevins as they migrate from the subsurface to flowing water [e.g., *Kondolf*, 2000; *May et al.*, 2009]. It is thus important to predict the mobile bed conditions associated with different augmentation strategies, given the regulated flow regime and the geomorphic constraints.

[7] We have used the tool presented here to specifically investigate the effects that gravel augmentations may have in the regulated reach of the Trinity River. In this reach, sedimentation of fine sediment is one of the major risks to salmon egg and embryo survival because it can cause a reduction in the intergravel flow, with a consequent trapping of the young fish that try to emerge from the gravel [*May et al.*, 2009]. In particular, the application we present here proceeded in four successive steps. We first applied the model to reconstruct conditions of mobile bed equilibrium for the unregulated Trinity River. This process included steps 1 and 2, i.e., the zeroing and test runs, respectively, presented in sections 4.1 and 4.2, respectively. In step 3, we used the numerical model to make predictions for conditions of nonequilibrium flow. In particular, we focused on the regulated period from the closure of the dams in 1962–2004, when controlled flow releases from the dams started. This step then consists of the postdam runs. Finally, in the augmentation runs of step 4 we predicted the effects of 120 years of gravel augmentation, considering two augmentation rates and two different grain size distributions of the added gravel.

[8] The methodology applied in sections 2.3, 4.3, and 4.4 to evaluate the quality of the spawning gravel is that proposed by *Kondolf* [2000]. The analysis is done in two steps: it is first required that the gravel is fine enough to be mobilized by spawning fish. The fractions of sediment finer than 1, 3, and 6 mm are then compared with the "thresholds for fine sediment content" given by *Kondolf* [2000].

[9] The organization of the paper is as follows. A description of the modeled stretch of the Trinity River is presented to justify the input parameters of the numerical runs and to introduce places and names that are referred to in the following sections. The numerical model is then described. Finally, the numerical results obtained by application of the model to the Trinity River are presented and discussed.

[10] In the text below, the terms "sediment transport rate" and "bed load input rate" (i.e., the sediment contributed from the basin to the river) specifically refer to the transport and the input rates of channel bed sediment only. Finer fractions that are simply transported downstream with little interaction with the bed are not considered in the mass balance and in the computation of the bed load transport rate and its grain size distribution.

## 2. Study Area

[11] The Trinity River is the largest tributary of the Klamath River in northwest California. It originates in the Scott Mountains and Trinity Alps of northern California, approximately 96 km upstream of Trinity Dam (see Figure 1). The regulated main stem Trinity River downstream of Trinity Dam is approximately 180 km long. It receives water and sediment from several tributaries and joins the Klamath River 70 km upstream of where it flows into the Pacific Ocean. The Trinity River watershed, excluding the South Fork, has a drainage area of 5271 $km^2$ in a sparsely populated and mountainous area with elevations ranging between 90 m at the confluence with the Klamath River and more than 2740 m in the Trinity Alps [*Graham Matthews and Associates*, 2001]. The climate is characterized by dry summers and wet winters. High-elevation headwater

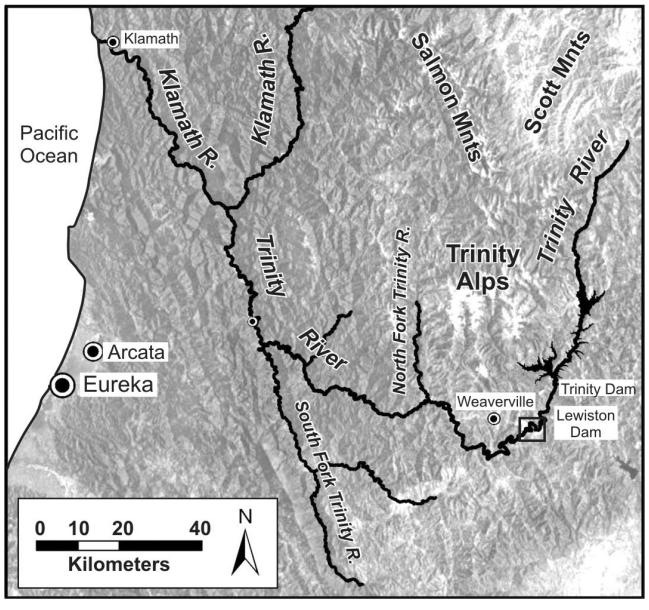


**Figure 1.** Basin of the Trinity River, northern California, latitude 41°N, longitude 123°W. The small box denotes the modeled reach represented in Figure 2.

areas in the mountains accumulate deep winter snowpacks that occasionally contribute to large, short-duration floods when warm Pacific storms produce intense rain-on-snow events in a weather pattern locally known as the pineapple express.

[12] Few quantitative data are available to reconstruct the geomorphologic attributes of the predam Trinity River, which are primarily inferred from aerial photographs and anecdotal accounts. In addition, conditions prior to European settlement are essentially unknown because the area was massively disturbed by gold mining and other human activities since the mid-1800s. Mining activities in the second half of the nineteenth century used hydraulic cannons to placer mine entire mountain sides, inundating the main valleys with large quantities of sediment. Upslope hydraulic mining continued well into the twentieth century (e.g., the La Grange mine), while most of the main stem valley floor was being excavated and inverted by dredge mining. Extensive and poorly managed timber harvesting beginning in the second half of the 1800s and continuing into the 1980s also contributed to high sediment production rates.

[13] In 1955 the U.S. Congress authorized the construction of the Trinity River Diversion to divert water from the Trinity River Basin in northern California to the Sacramento River Basin and the Central Valley for the development of agricultural activities. The system consists of two dams: Trinity Dam upstream and Lewiston Dam, approximately 13 km downstream. Trinity Dam stores and regulates the flow for water supply, irrigation, and production of electrical energy. Lewiston Dam is smaller and was built to regulate the releases into the Trinity River and the diversion to the Central Valley.

[14] Construction work ended in 1962; up to 90% of the runoff from upstream of the dams was diverted to the Central Valley for the next decade. A very narrow flow discharge range from 4 to 8 $m^3 s^{-1}$ was released from Lewiston Dam to the reach under study. This range was chosen on the basis of a recommendation dating from the original project design, according to which an annual release volume of 149 million $m^3$ would be sufficient to maintain the fish and the wildlife habitat below the dams [*U.S. Fish and Wildlife Service and Hoopa Valley Tribe*, 1999].

[15] Although its watershed has been intensively modified by human activities since the second half of the 1800s, the predam Trinity supported a vigorous commercial salmon and steelhead fishery [*Moffett and Smith*, 1950; *Nelson et al.*, 1987] that declined dramatically after a decade of regulated flow. Since the 1970s, it has been recognized that an increase in the annual released volume is necessary to establish an appropriate flow regime for fish and other species in the regulated part of the river. In December 2000 the Secretary of the Interior adopted the Record of Decision (ROD) to regulate in-stream flow releases. Five different hydrographs were defined to encompass a range of seasonal and interannual flows believed to be suitable for environmental rehabilitation depending on the classification of the water year (i.e., extremely wet, wet, normal, dry, and critically dry).

### 2.1. Modeled Stretch

[16] The modeled stretch of the Trinity River starts at the confluence with Deadwood Creek (river kilometer 179) and ends at the confluence with Grass Valley Creek (approximately river kilometer 167). Figure 2 shows a map from Lewiston Dam to Grass Valley Creek, along with the two tributaries with Deadwood and Rush Creek and the U.S. Geological Survey (USGS) gauging station at Lewiston. This part of the river was selected because its proximity to the dam means that the effects of flow regulation and the loss of the upstream coarse-sediment supply are more evident here than farther downstream where the accretion of water and sediment from tributaries becomes significant. In addition, specification of tributary sediment inputs becomes

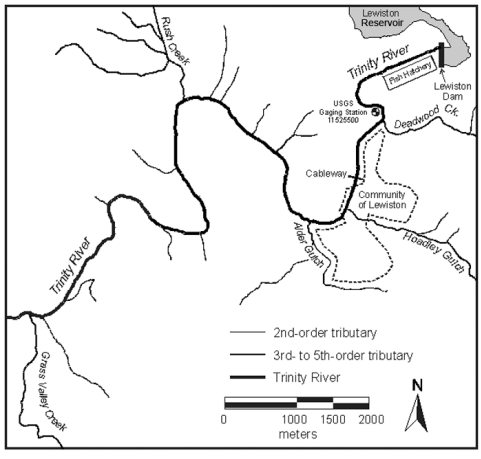


**Figure 2.** Modeled reach of the Trinity River.

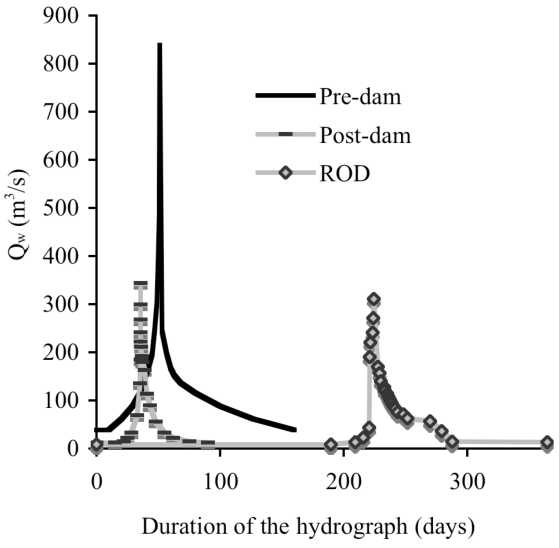


**Figure 3.** Cycled repeated hydrographs. For predam (1911–1959) and postdam (1962–2004) hydrographs it is assumed that the river was morphologically active for only part of the year. The Record Of Decision (ROD) hydrographs accounts for all the released discharges.

increasingly uncertain downstream as the number of potential sediment sources increases.

[17] It can be seen from Figure 2 that Rush Creek is the only major tributary within the study reach. It is assumed in the remainder of this paper that the effect of Rush Creek and lower-order tributaries can be ignored in modeling predam conditions but must be included in modeling postdam conditions. The area of the drainage basin upstream of Lewiston Dam is so large (1861 $km^2$) that under predam conditions, the additional water and sediment from Rush Creek is modest enough to be ignored. This assumption was used for the zeroing and test runs. On the contrary, for postdam simulations the modeled domain has been divided into two segments, one upstream and one downstream of Rush Creek, because the increase in sediment supply due to Rush Creek is no longer negligible. These segments are as follows.

[18] 1. The Lewiston segment extends from the confluence with Deadwood Creek to the confluence with Rush Creek (river kilometer 174), where a delta of coarse sediment produces a low-gradient backwater profile extending approximately 0.5 km upstream at base flow. Deadwood Creek drains a basin of 23 $km^2$; its bed material is made up of coarse gravel and cobbles. Since the 1970s, gravel augmentations have been performed in this segment in an attempt to reduce the characteristic size of the very coarse surface layer that is one of the major causes of the decline of the salmonid population [*U.S. Fish and Wildlife Service and Hoopa Valley Tribe*, 1999].

[19] 2. The Bucktail/Lowden segment extends from Rush Creek to the confluence with Grass Valley Creek. Rush Creek is a perennial tributary that drains an area of 58.5 $km^2$.

### 2.2. Hydrology

[20] Hydrological data are recorded at the USGS gauging station at Lewiston. Daily mean discharges and peak streamflows are available since water year (WY, i.e., from 1 October of the previous calendar year to 30 September) 1911. These data have been used to define predam (1911–1959) and postdam (1961–2004) input hydrographs (Figure 3).

[21] Predam streamflows in the Trinity River were highly variable: summer flows at the Lewiston stream gauge less than 3 $m^3$ were not uncommon, whereas the predam 2 year peak flow was about 450 $m^3\ s^{-1}$ and the instantaneous peak of record was 2027 $m^3\ s^{-1}$ on 22 December 1955. In addition to the winter storm peaks, predam Trinity hydrology also included a longer-duration annual snowmelt hydrograph lasting several weeks between March and July, with daily average peak flow generally between 120 and 320 $m^3\ s^{-1}$. In wet years the peak snowmelt occurred later in spring than in dry years.

[22] The hydrographs in Figure 3 represent simplifications of the flow duration curve based on daily flows in that the discharges in the former have been ordered so that they begin with a low discharge, monotonically increase to a maximum discharge, and then monotonically decrease to a low end discharge.

[23] The postdam input hydrograph for both model segments was derived from the flow duration curve for the USGS gauging station at Lewiston from 1962 to 2004. It thus incorporates the full range of discharge magnitudes and durations recorded at the Lewiston gauge during the postdam period, even though it does not reproduce the historical time series of streamflow.

[24] The validity of neglecting tributary inputs downstream from the Lewiston gauge for modeling postdam conditions was evaluated by comparing mean annual flows at the Lewiston gauge with those measured at the USGS Trinity River stream gauge below Limekiln Gulch (USGS 11525655), which is located about 8 km downstream from the downstream boundary of the Bucktail/Lowden segment. The average annual discharge record at the Limekiln Gulch gauge overlaps with that of the Lewiston gauge in 17 years of the postdam period through WY 2009. During those years, the mean discharge at Limekiln Gulch was 12.8% greater than the mean discharge at Lewiston. However, about 55% of the tributary area contributing to accretions

at Limekiln Gulch is located downstream from the Bucktail/Lowden modeling segment, such that tributary inputs in that segment represent less than 6% of the discharges recorded at Lewiston.

### 2.3. Grain Size Distribution of the Bed Surface and of the Substrate

[25] An average grain size distribution of the substrate for both predam and postdam numerical runs was estimated by compiling subsurface bulk samples of spawning gravel taken in the fall of 2000. Two bulk substrate samples were obtained at each of six locations in the Trinity River ranging from 6 to 50 km downstream from Lewiston Dam, using a 0.6 m diameter McNeil-type sampler [*Graham Matthews and Associates*, 2001]. The sampling cylinder was worked into the bed, and the surface layer, defined as the depth of the largest surface particle, was removed. The remaining substrate material in the sampler was then excavated to a depth of approximately 0.4 m and wet sieved. Particles larger than 16 mm were wet sieved in rocker boxes in the field, whereas the finer material was taken to the laboratory for analysis. Substrate samples collected at two additional locations by *Graham Matthews and Associates* [2001] were deemed unrepresentative of the prevailing substrate conditions and were excluded from this analysis. One of these sample locations is immediately downstream from the Lewiston Dam spillway, in an area that has been altered by artificial gravel augmentations and winnowing of the sand and smaller gravel fractions since dam closure. The other excluded sample location was situated in an area of local sand deposition, where the sediment was clearly much finer than of the bed through the majority of the modeling domain. In the absence of predam substrate data, the average subsurface particle size distribution, shown in Figure 4 with all the substrate samples mentioned, is assumed to also represent the predam substrate. This assumption is based on the assumption that postdam regulated flow magnitudes have generally been insufficient to scour the bed to appreciable depths and alter the subsurface composition. We nonetheless recognize that fine sediments may have infiltrated into the voids of the substrate under postdam flow and sediment transport conditions, even though the gravel matrix itself may be undisturbed. Therefore, the predam substrate may well have contained a smaller fraction of sand-sized sediments than is shown in Figure 4.

[26] Applying the methodology proposed by *Kondolf* [2000], it was found that for a median diameter of the spawning gravel of 20 mm, the length of the spawning salmonid should be larger than 150–200 mm [*Kondolf*, 2000, Figure 4]. The salmonid population in the predam Trinity River consisted mostly of chinook and coho salmon and steelhead (or rainbow) trout that are generally longer than 200 mm [*Kondolf and Wolman*, 1993]. The analysis of the fine sediment reveals that in the (assumed) predam substrate the fractions of sediment finer than 1, 3, and 6 mm are 7%, 20%, and 29%, respectively. According to *Kondolf* [2000, Table 1] the maximum content for these sediment sizes in a healthy spawning gravel for the salmonid species considered in the present study should be, on average, smaller than 13%, 25%–30%, and 30%, respectively (with a minimum of 16% and a maximum of 40% for the coarsest fraction). The content of sediment finer than 6 mm in the assumed predam substrate is close to the maximum limit; this may be a consequence of postdam infiltration of fine sediment during the regulated period.

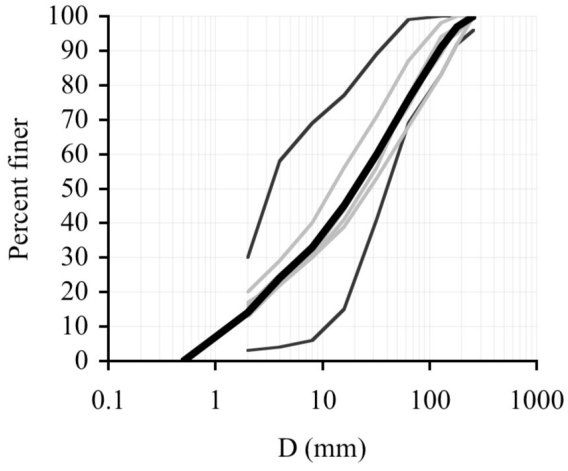


**Figure 4.** Grain size distribution of the Trinity River subsurface determined from bulk samples collected at six locations in 2001. The thin dark gray lines are samples considered to be unrepresentative of the substrate. The thin light gray lines are the samples used in the calculation of the average substrate, which is represented by the thick black line. Characteristic parameters of the average substrate are geometric mean diameter $D_g = 16$ mm, median diameter $D_{50} = 20.2$ mm, diameter such that the 90% of the sediment is finer $D_{90} = 122.2$ mm, and the geometric standard deviation $\sigma_g = 5.13$.

[27] The size distributions of bed surface in the predam period and just after the closure of the dams (i.e., initial condition for the postdam numerical runs) are also unknown. Therefore, in numerical runs used to "zero" the model so as to characterize predam, equilibrium conditions, it was initially set equal to that of the substrate, and the model was run until a coarser, quasi-equilibrium bed surface developed. This assumed initial condition does not affect the numerical results at mobile bed equilibrium because in a sediment feed flume they are independent of the initial conditions (i.e., initial longitudinal profile and grain size distribution of the bed surface and of the substrate) [*Parker and Wilcock*, 1993].

[28] For the postdam runs, initial grain size distribution of the bed surface must be chosen carefully to properly reproduce the variation of the channel bed over 42 years of regulated flow (from 1962 to 2004). This is because over the period in question, the model is applied to a river that is not in equilibrium and so the results are strongly dependent on the initial conditions. Unfortunately, the grain size distribution of the bed surface of the predam Trinity River is unknown, so two different initial conditions have been hypothesized: (1) the default of a bed surface that has the same size distribution as the substrate and (2) a bed surface that has the coarser size distribution associated with the quasi–equilibrium obtained in the zeroing runs. These conditions are discussed in more detail in section 4.3.

[29] The median surface size $D_{s50}$ and the surface size $D_{s90}$ (i.e., diameter of the bed surface such that 90% of the

**Table 1.** Characteristics of the Zeroing Runs[a]

| Run | $\tau^*_{ssrg}$ | $a_{trans}$ | $Q_{feed}$ (t yr$^{-1}$) | $S$ (m m$^{-1}$) | $L_{hbl}$ (m) | $D_{sg}$ (mmol) | $D_{s50}$ (mmol) | $D_{s90}$ (mmol) |
|---|---|---|---|---|---|---|---|---|
| Z1 | $\tau^*_{ssrg,Eq.(12)}$ | 0.2 | 16,199 | 0.0053 | 3000 | 88 | 139 | 227 |
| Z2 | $0.5\tau^*_{ssrg,Eq.(12)}$ | 0.2 | 16,199 | 0.0023 | 4500 | 81 | 136 | 226 |
| Z3 | $\tau^*_{ssrg,Eq.(12)}$ | 0.2 | 31,850 | 0.0058 | 4500 | 83 | 137 | 226 |
| Z4 | $0.5\tau^*_{ssrg,Eq.(12)}$ | 0.2 | 31,850 | 0.0025 | 4500 | 76 | 133 | 225 |
| Z5 | $0.5\tau^*_{ssrg,Eq.(12)}$ | 0.4 | 31,850 | 0.0025 | 4500 | 76 | 133 | 225 |
| Z6 | $0.5\tau^*_{ssrg,Eq.(12)}$ | 0.6 | 31,850 | 0.0025 | 4500 | 76 | 133 | 224 |

[a]Here $\tau^*_{ssrg}$ denotes the reference Shields number in the load relation, $a_{trans}$ denotes the parameter governing the grain size distribution of the material transferred to the substrate when the bed aggrades, $Q_{feed}$ denotes the sediment feed rate, and $S$ is the bed slope at equilibrium. Characteristic diameters of the bed surface at equilibrium are also reported: $D_{sg}$ denotes the geometric mean diameter, $D_{s50}$ is the median diameter, and $D_{s90}$ is the diameter such that the 90% of the sediment is finer. In addition, $\tau^*_{ssrg,Eq.(12)}$ denotes the value of $\tau^*_{ssrg}$ predicted by equation (12).

sediment is finer) of the current bed surface have been estimated from surface facies mapping in 2006 and 2007. These maps consisted of spatially continuous visual estimates of $D_{s50}$ and $D_{s90}$ particle sizes on the bed surface in local areas, such as riffle crests, pools, pool tail outs, and runs covering both modeled river segments. The average value of $D_{s50}$ throughout the domain in question was found to be about 90 mm, and the average $D_{s90}$ was 198 mm. Analysis of facies maps drafted independently by P. Wilcock (personal communication, 2003) gives similar results. These $D_{s50}$ and $D_{s90}$ values are assumed to be representative of the bed surface in 2004. They are compared with postdam numerical results herein, and in addition, they have been used to estimate a reasonable initial grain size distribution of the bed surface for the augmentation runs, as described in section 2.4.

### 2.4. Mean Annual Input Rate of Channel Bed Sediment and Its Grain Size Distribution

[30] The annual quantities and size distributions of bed load transported past the Lewiston dam site prior to dam construction are unknown. Because of the large uncertainties in estimating those parameters, two different approaches, based on the results of the field analysis conducted by *Graham Matthew and Associates* [2001, 2006], were used to bracket a reasonable range of values. That is, one estimate is derived from measured deposition rates in Trinity Lake, and the other is based on measurements of bed load and suspended load at Lewiston recorded in the 1950s.

[31] Surveys of delta growth at the mouths of three tributaries that flow into Trinity Lake provide an estimate of sediment delivery to the Trinity River as well as unregulated sediment fluxes in the main stem near Lewiston. Sediment input rates were estimated by *Graham Matthews and Associates* [2006] by comparing the bathymetry of the deltas of Stuart Fork, Mule Creek, and East Stuart Fork (Figure 5) with detailed maps that the Bureau of Reclamation prepared before the construction of the dams in 1957. Bathymetric measurements of the Stuart Fork delta were performed in 2001, whereas the other two deltas were surveyed in 2005. It is assumed that delta deposition started with the onset of flow regulation in 1961. After differencing the recent delta surveys with the predam topography, *Graham Matthews and Associates* [2006] converted the volume fill to weight (using 1.26 t m$^{-3}$) and multiplied by 1.2 to account for an estimated 80% trap efficiency in the delta. The resulting total sediment delivery quantities were divided by the number of years between 1961 and the survey dates and by contributing area to yield the annual unit sediment delivery rate to the three deltas. We then computed a total annual sediment delivery rate to the Trinity Dam site of 131 t km$^{-2}$ yr$^{-1}$ as the area-weighted average of the delivery rates to the three deltas. Alternatively, a mean annual sediment yield for the unregulated Trinity River at Lewiston of 58 t km$^{-2}$ yr$^{-1}$ was obtained from field measurements of suspended sediment performed in the 1950s and 1960s [*Knott*, 1974].

[32] We converted these two estimates of total sediment yield from the upper Trinity basin to bed load sediment

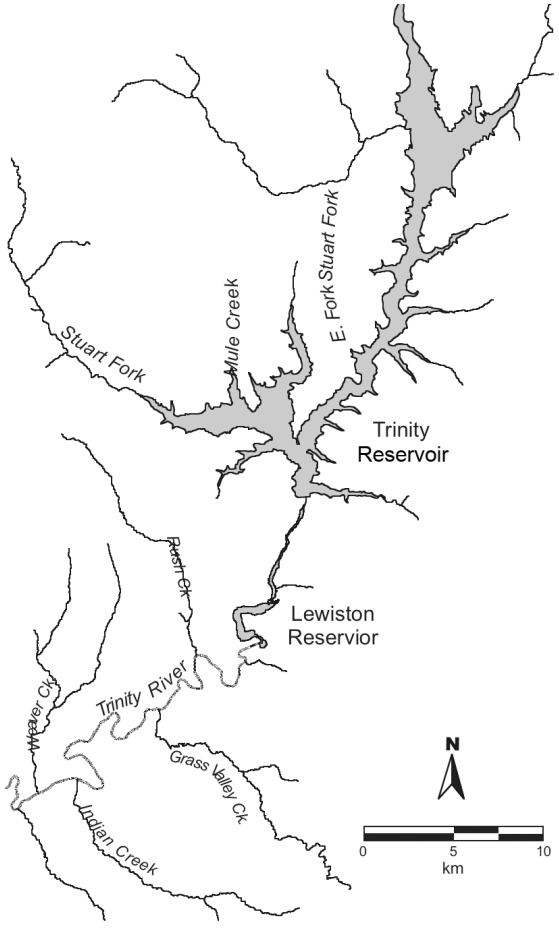


**Figure 5.** Trinity Lake and its tributary arms where deltas were surveyed.

yield by assuming that bed load comprises about 15% of the suspended sediment load [*Graham Matthews and Associates*, 2006]. This resulted in the following bounds for the mean annual bed load yield to the Trinity River at Lewiston: 17 t $km^{-2}$ $yr^{-1}$, corresponding to a bed load input rate of 31,850 t $yr^{-1}$, and 8.7 t $km^{-2}$ $yr^{-1}$, corresponding to a bed load input rate of 16,199 t $yr^{-1}$.

[33] The grain size distribution of the predam sediment supply is assumed to be equal to the average grain size distribution of the substrate. This assumption can be partially justified considering that the strong form of equal mobility for the transport of gravel is generally observed in higher-order gravel bed rivers [*Parker and Toro-Escobar*, 2002].

[34] Postdam bed load input rates in the modeled reach are equal to the sum of the bed material load delivered from the tributaries and that from artificial gravel augmentations because all the sediment contributed from the basin upstream of the dam is trapped in the reservoirs. Bed load input rates are separately computed for the Lewiston and for the Bucktail/Lowden segments.

[35] Annual sediment yields contributed from tributaries were estimated using several different methods. For Deadwood and Rush Creeks, fractional and total bed load rating curves and flow duration curves were developed using the available bed load transport measurements and streamflow data [*Gaeuman*, 2008a]. These analyses resulted in estimated average annual bed load inputs of 273 t $yr^{-1}$ from Deadwood Creek and 651 t $yr^{-1}$ from Rush Creek. The unit bed load yield computed for Rush Creek was assumed to be valid for other small, ungauged tributaries draining the area river right of the main stem, which is broadly underlain by similar geology to that found in the Rush Creek basin [*Gaeuman*, 2008a]. The tributary area river left of the main stem and downstream from the Deadwood Creek basin predominantly drains lands underlain by decomposed granites that produce copious quantities of sand and very fine gravel [*Lisle and Hilton*, 1992; *Wilcock et al.*, 1996]. *Gaeuman* [2008a] estimated the unit bed load yield from those areas on the basis of dredge records at Hamilton and Wellock ponds, as reported by *Trso* [2004]. These ponds, which are located at the confluence of Grass Valley Creek with the Trinity River, have been dredged about every other year since 1984 in an effort to prevent the delivery of sand-sized sediments to the Trinity River. These analyses produced total estimated bed load inputs from ungauged tributaries to the right of the main stem of 115 t $yr^{-1}$ of coarse sand and fine gravel, with the same grain size distribution as the bed load contributed from Rush Creek from the right side of the main stem (Figure 6a). They also resulted in an estimated input of 3307 t $yr^{-1}$

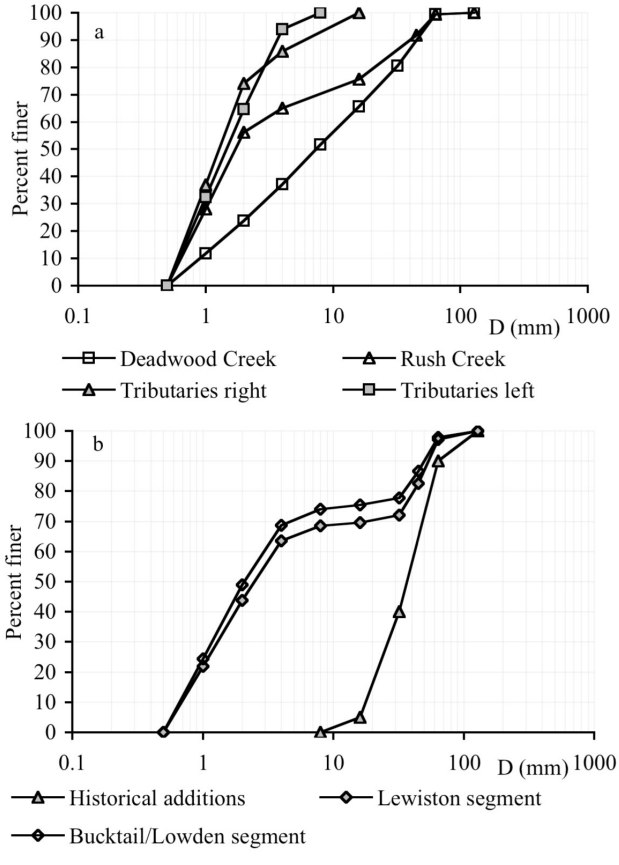


**Figure 6.** Grain size distributions of (a) bed load inputs from Deadwood Creek, Rush Creek, and the ungauged tributaries on the left and right sides of the main stem and (b) gravel augmentations (1961–2004) and tributary bed load inputs in the Lewiston and Bucktail/Lowden segments.

of predominantly fine bed load (<8 mm) −8 mm from the left side of the main stem (Figure 6a). One quarter of the ungauged right-side bed load input and three fourths of the ungauged left-side bed load inputs were assigned to the Lewiston modeling segment according the fractions of the ungauged right- and left-side areas' tributary to that segment, and the remaining fractions were assigned to the Bucktail/Lowden segment [*Gaeuman*, 2008a].

[36] The mean annual rate of gravel augmentation downstream from Lewiston Dam during the modeled period (1961–2004) was determined by dividing the total volume of coarse sediment added prior to 2004 by the duration of the simulation (42 years). According to a review of augmentation records by *Kondolf and Minear* [2004], a total of 46,405 t of material was added during that time frame, for a mean annual input rate of 1079 t $yr^{-1}$. Summary grain size statistics given by *Kondolf and Minear* [2004] suggest that the typical grain size distribution of the added material was approximately as shown in Figure 6b.

[37] The estimated mean annual bed load input rate for the Lewiston segment is the sum of the input rate from Deadwood Creek, the ungauged tributaries, and the gravel augmentations, which have mostly been done between Lewiston Dam and the confluence with Deadwood Creek, i.e., 3861 t $yr^{-1}$. The mean annual bed load input rate for the Bucktail/Lowden segment is 5425 t $yr^{-1}$, i.e., the sum of the input rates for the Lewiston segment, the mean annual bed load input rates of Rush Creek, and ungauged tributaries. The grain size distributions of the bed load input rates to the modeled segments are also presented in Figure 6b.

## 3. Numerical Model

[38] The model has the same structure of that described by *Parker et al.* [2008]: the sediment is considered to be a mixture of different grain sizes, and the river is modeled in analogy to a sediment feed flume. That is, a cycled annual hydrograph, as well as the sediment feed rate and grain size distribution are user-specified parameters. The sediment feed rate is held constant over the hydrograph; as shown by *Parker et al.* [2008] and *Wong and Parker* [2006], the sediment transport rate evolves to follow the hydrograph only a short distance downstream of the feed point.

[39] In principle, the model can handle a sediment transport rate that varies with flow discharge, but this would require a detailed sediment budget that is beyond the scopes of the present work. The evolution in time and space of the longitudinal profile of the river is computed by imposing the conservation of channel bed sediment (i.e., Exner equation).

[40] In the model reported here, (1) the cross section is assumed to be rectangular, but its width is allowed to vary with the flow discharge, and (2) a procedure to store and access the stratigraphy of the bed deposit [*Viparelli et al.*, 2010] is implemented to investigate the effects that a variation in magnitude and grain size distribution of the sediment supply may have on the bed surface and the topmost part of the substrate (i.e., the area where fish spawn). The interaction between the bed load and the channel bed is modeled with the active layer approximation [*Hirano*, 1971], as modified by *Parker* [1991a, 1991b]. The bed is divided into two layers: the active layer and the substrate. The active layer occupies the upper part of the bed; it has no vertical structure, and all particles of a given size have the same finite probability to be entrained into bed load. The substrate is the entire bed under the active layer; it may show a vertical stratigraphic variation (variation of the grain size distribution in the vertical), but the particles cannot be directly entrained into bed load [*Parker*, 1991a]. The grain size distribution of the substrate may vary as the bed aggrades or degrades because aggradation transfers active layer material to the substrate and degradation does the opposite.

[41] Here the topmost part of the substrate represents a region of the substrate just below the bed surface, where spawning fish deliver their eggs. This layer is assumed to be approximately 1 m in the calculations presented in section 4.

[42] Even with an imposed cycled hydrograph in a gravel bed stream, it is still possible to define a condition of mobile bed equilibrium, under which the bed load transport rate and its grain size distribution vary cyclically with the flow discharge, but bed elevation and the grain size distribution of the bed surface have adjusted to change only modestly over the hydrograph [*Parker et al.*, 2008; *Wong and Parker*, 2006]. When the flow and the sediment transport reach a condition of mobile bed equilibrium, the values of all the hydraulic parameters (e.g., channel slope and total bed load transport rate) averaged over the entire hydrograph are constant in time and space. As noted, this mobile bed equilibrium is reached downstream of a relatively short (compared to the total length of the domain) region in the upstream part of the channel that has been called the hydrograph boundary layer [*Parker et al.*, 2008; *Wong and Parker*, 2006].

[43] The river reach is divided into $M$ computational nodes. Given (1) the input hydrograph feed rate and grain size distribution and (2) the longitudinal profiles of elevation and grain size distribution of the bed at some time $t$, water depth, bed shear stress, and bed load transport rate are computed in each node assuming a rectangular cross section of variable width. The equation of conservation of channel bed sediment is then solved to compute the new longitudinal profile as well as the new grain size distribution of the bed surface at time $t + \Delta t$ [*Parker*, 1991a]. This loop is then repeated to step forward in time.

[44] Essential features of the model include the following. (1) A description of the interannual variability of the water discharges is specified in terms of a repeated annual hydrograph. (2) The width of the rectangular cross section is assumed to vary with the water discharge so as to capture the variation of at-a-station hydraulic geometry. (3) The procedure of *Viparelli et al.* [2010] to store and access deposit stratigraphy as the bed aggrades/degrades is implemented.

[45] The governing system of differential equations is solved with the same numerical scheme as that proposed by *Parker et al.* [2008]. The spatial derivatives of a function $f$ at node $i$ are computed as

$$\left.\frac{\partial f}{\partial x}\right|_i = a_u \frac{f_i - f_{i-1}}{\Delta x} + (1 - a_u)\frac{f_{i+1} - f_i}{\Delta x}, \qquad (1)$$

where $\Delta x$ is the spatial step length and $a_u$ is an upwinding coefficient set equal to 0.75 in the numerical runs described in the next paragraph.

[46] In the model, it is assumed that small-scale bed forms are absent, and the active layer thickness $L_a$ is evaluated as a linear function of $D_{s90}$:

$$L_a = n_a D_{s90}\,, \tag{2}$$

where $n_a$ is a user-specified parameter that has been estimated to vary between 1 and 2 (G. Parker, 1D sediment transport morphodynamics with applications to rivers and turbidity currents, e-book, 2004, available at http://vtchl.uiuc.edu/people/parkerg/, hereafter referred to as Parker, e-book, 2004). In the present runs, $L_a$ has been set equal to 2.

### 3.1. Input Hydrograph

[47] The input hydrograph is divided in a series of $N_{\text{disc}}$ constant water discharges of duration $\Delta t_w$. The river is considered to be morphologically inactive when it is not in flood (Parker, e-book, 2004). To calculate bed evolution during a flood, a time step for flood conditions $\Delta t_f$ that can be smaller than the time step $\Delta t_w$ must be specified. The relation between $\Delta t_w$ and $\Delta t_f$ is

$$\Delta t_w = n_{\text{step}} \Delta t_f\,, \tag{3}$$

where $n_{\text{step}}$ represents the number of time steps for which calculations are performed for each value of flow discharge. In the numerical runs described in section 4, $\Delta t_f$ was equal to half a day, and $n_{\text{step}}$ varied between 0.2 and 66.

[48] When water discharge is expressed as an input hydrograph, its evolution in the downstream direction should be considered. In a relatively short reach of a gravel bed stream without major tributaries, the variation of the hydrograph can be reasonably neglected, and it is assumed that the discharge is the same in each node (Parker, e-book, 2004).

[49] In modeling the hydraulics of the river, the normal flow is assumed, and the water depth at each node is computed with a Manning–Strickler formulation:

$$H = \left(\frac{q_w^2 k_s^{1/3}}{\alpha_r^2 g S}\right)^{3/10}, \tag{4}$$

where $\alpha_r$ is a coefficient set equal to 8.1 in the numerical runs [*Parker*, 1991b], $g$ is the acceleration of gravity, $S$ is the bed slope, $q_w$ is the water discharge per unit width, and $k_s$ is the roughness height evaluated as linear function of the $D_{s90}$,

$$k_s = n_k D_{s90}\,. \tag{5}$$

[50] Here $n_k$ is a user-specified parameter that may vary between 2 and 3 (Parker, e-book, 2004); it is assumed to be 2 in the numerical simulations reported here.

### 3.2. Width-Discharge Relation

[51] Variation of the width of the rectangular cross section $B$ with the flow discharge $Q_w$ is described with a function of the form

$$\frac{B}{B_{\text{ref}}} = \left(\frac{Q_w}{Q_{w\text{ref}}}\right)^n, \tag{6}$$

where $B_{\text{ref}}$ and $Q_{w\text{ref}}$ denote the reference values of channel width and water discharge, respectively. In particular, for the predam Trinity River the reference discharge is assumed to be the peak flood with a 2 year recurrence frequency, i.e., 368 $m^3$ $s^{-1}$, and the reference width is assumed equal to 84 m on the basis of rather sparse field data. For the regulated period, the reference values of channel width and water discharge are equal to 40 m and 24 $m^3$ $s^{-1}$, respectively. The reference discharge used under postdam conditions is a nominal one based on prevailing low-flow conditions, while the reference width is the width of the channel between the vegetated banks, as measured in the field and from the 2006 aerial photographs.

[52] Predam and postdam values for the exponent $n$ in equation (6) have been determined by plotting water discharges recorded at the USGS station at Lewiston and channel widths measured on the same day, as reported in Figure 7. The width data have been recorded at the Cableway (see Figure 2). This section is typical for the postdam Trinity River, as documented by recent field observations, but whether or not it is a good representation of the predam river remains open to question. This issue could not be properly resolved in the absence of more field data.

[53] The measured widths are assumed to be equal to the width of the modeled rectangular cross section. This approximation is reasonable for the present river, which is characterized by an almost-rectangular cross section, as documented by repeated surveys and *U.S. Fish and Wildlife Service and Hoopa Valley Tribe* [1999]. It could have been revisited for the unregulated river were more field data available.

[54] The exponent $n$ in equation (6) for the predam Trinity River was found to be equal to 0.09, while it was found to be equal to 0.31 for the regulated river. Here we assume it to be constant over the entire modeled domain.

[55] The channel width estimated from equation (6) is then used in the calculation of the flow, the sediment transport, and the morphodynamic evolution of the river. It could be argued that for the sediment calculations a depositional area wider than the channel should have been considered to account for the overbank deposition of sediment when the river is in flood. Considering that the present

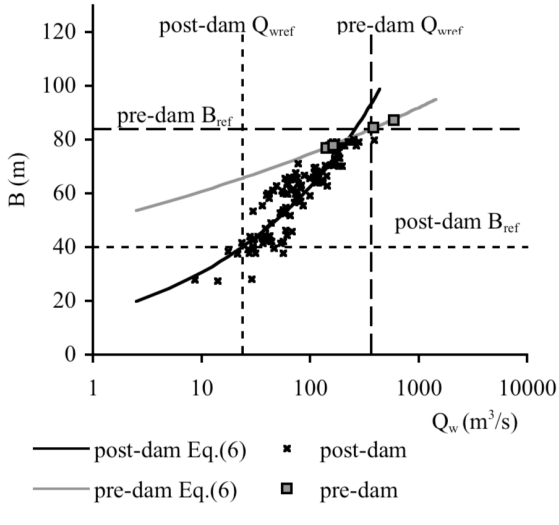


**Figure 7.** Width-discharge relations.

model considers channel bed material that is transported as bed load only, the width considered for the conservation of sediment has been set equal to the channel width.

### 3.3. Bed Load Transport Relation

[56] The bed load transport relation for sediment mixtures is that of *Wilcock and Crowe* [2003]. The total bed load transport rate per unit width $q_{bT}$ is defined as the sum of the bed load transport rates of each grain size $q_{bi}$. The fraction of bed load material in the $i$th grain size range $p_i$ is defined as

$$p_i = \frac{q_{bi}}{q_{bT}} . \tag{7}$$

[57] The bed load transport rate per unit width in each grain size range $q_{bi}$ is computed as

$$q_{bi} = \frac{u_*^3}{Rg} F_i W_i^* , \tag{8}$$

where $R$ is the specific gravity of the sediment, defined as $(\rho_s - \rho)/\rho$, where $\rho_s$ is the density of the sediment and $\rho$ is the density of water; $F_i$ is the fraction of material of the surface layer in the $i$th grain size range; $u_*$ is the shear velocity; and $W_i^*$ is a nondimensional parameter herein called the grain size-specific bed load transport rate. In addition, $u_*$ denotes the shear velocity, defined as

$$u_* = \sqrt{RgD_{sg}\tau_{sg}^*} , \tag{9}$$

where $D_{sg}$ is the geometric mean diameter of the surface layer and $\tau_{sg}^*$ denotes the relevant Shields parameter characterizing bed mobility. For the normal flow conditions assumed here, this parameter can be estimated as

$$\tau_{sg}^* = \frac{HS}{RD_{sg}} . \tag{10}$$

[58] The grain size–specific bed load transport rate $W_i^*$ is computed as a function of the parameter $\phi_i$:

$$\phi_i = \frac{\tau_{sg}^*}{\tau_{ssrg}^*}\left(\frac{D_i}{D_{sg}}\right)^{-b}, \; W_i^* = G(\phi_i) , \tag{11}$$

where $D_i$ is the characteristic diameter of the $i$th grain size range, $\tau_{ssrg}^*$ is a reference value for the Shields parameter computed as a function of the fraction of sand in the active layer $F_s$ using

$$\tau_{ssrg}^* = 0.021 + 0.015\exp(-20F_s) , \tag{12}$$

and the exponent $b$ is a function of the ratio between the characteristic diameter of a given grain size range $D_i$ and the surface geometric mean diameter,

$$b = \frac{0.67}{1 + \exp\left(1.5 - D_i/D_{sg}\right)} . \tag{13}$$

[59] The function $G(\phi_i)$ is further defined as

$$G(\phi_i) = \begin{cases} 0.002\phi_i^{7.5}, & \phi_i < 1.35, \\ 14\left(1 - \frac{0.894}{\phi_i^{0.5}}\right)^{4.5}, & \phi_i \geq 1.35. \end{cases} \tag{14}$$

[60] As discussed in section 4.1, in the numerical runs the reference value of the Shields number has been adjusted downward in order to predict a channel slope at equilibrium for the unregulated Trinity River that is close to the present slope of the river.

### 3.4. Mass Conservation for Sediment

[61] The standard form of the Exner equation expressing the conservation of mass of sediment is

$$(1 - \lambda_p)\frac{\partial \eta}{\partial t} = -I_f \frac{\partial q_{bT}}{\partial x} , \tag{15}$$

where $\lambda_p$ is the bed porosity, $\eta$ is the bed elevation above a datum, $I_f$ represents the time that the river is morphologically active (e.g., Parker, e-book, 2004), $t$ denotes time, and $x$ denotes the streamwise coordinate. The factor $I_f$ has been introduced in order to have an input hydrograph shorter than 1 year with a total duration that is equal to the time that the river is morphologically active. In other words, it is assumed that low discharges unable to move a significant amount of sediment can be neglected.

[62] The grain size–specific form of the Exner equation is used to update the grain size distribution of the bed surface in each node as the bed aggrades/degrades [*Parker*, 1991a]:

$$(1 - \lambda_p)\left[L_a \frac{\partial F_i}{\partial t} + (F_i - f_{Ii})\frac{\partial L_a}{\partial t}\right] = -I_f \frac{\partial (q_{bT} p_i)}{\partial x} + I_f f_{Ii} \frac{\partial q_{bT}}{\partial x} . \tag{16}$$

[63] Here $f_{Ii}$ represents the fraction of material in the $i$th grain size range exchanged across the active layer–substrate interface as the bed aggrades or degrades. In an active layer formulation, a discontinuity in the grain size distribution may be present here. When the bed degrades, $f_{Ii}$ is assumed to be equal to the grain size distribution of the substrate, while during aggradation it is computed as a weighted average between the grain size distributions of the surface layer and the bed load [e.g., *Hoey and Ferguson*, 1994]:

$$f_{Ii} = a_{\text{trans}} F_i + (1 - a_{\text{trans}}) p_i . \tag{17}$$

[64] Here $a_{\text{trans}}$ is a parameter that varies between 0 and 1. It cannot be precisely unity because with this value the material in the active layer is directly transferred to the substrate and the coarsening of the surface layer observed in gravel bed rivers cannot be reproduced. On the other hand, it cannot be zero because if the bed load is directly transferred to the substrate, the downstream fining observed in many gravel bed rivers cannot be reproduced [*Toro-Escobar et al.*, 1996]. In the zeroing runs used to estimate a predam equilibrium state, this parameter has been calibrated so as to yield a

numerical substrate with an average grain size distribution similar to the present substrate.

### 3.5. Procedure to Store and Access the Stratigraphy

[65] To illustrate how the model stores and accesses the stratigraphy of the bed deposit, a grid has been drawn on the bed (Figure 8). This grid has a number of columns equal to the number of computational nodes $M$. The number of rows varies according to the elevation of the active layer–substrate interface in each node and the vertical thickness of the grid $L_s$ used to discretize the vertical variation in the substrate grain size distribution into a set of storage layers. [*Viparelli et al.*, 2010]. In the present model $L_s$ is a user-specified parameter that has been set equal to 1 m in all the present numerical simulations. A grain size distribution is associated with each point of the grid to represent the sediment stored in the layer below, as shown in Figure 8 (so that the grain size distribution associated with layer $k$ is representative of the layer between point $k-1$ and point $k$). In each column, the upper point of the grid is located at the active layer–substrate interface; this point follows the interface as the channel bed aggrades/degrades.

[66] When the bed aggrades, sediment is transferred to the substrate. The grain size distribution of this transferred sediment is given by equation (17). The fractions of sediment in each size range in the upper layer of the grid are computed as a weighted average over the thicknesses of the previous and newly deposited layers. When the distance between the upper two nodes of the grid becomes greater than $L_s$, a new row is added to the grid. The thickness of the old upper row of the grid then becomes equal to $L_s$, and a new storage layer is added with an upper elevation equal to the position of the new active layer-substrate interface. The grain size distribution associated with this new layer is given by equation (17).

[67] When the bed degrades, the upper point of the grid follows the active layer–substrate interface, and its grain size distribution does not change unless this upper point becomes lower than the bottom of a given storage layer. When this happens, the number of storage layers decreases, and the grain size distribution of the substrate sediment immediately below the surface layer is adjusted accordingly.

### 3.6. Initial and Boundary Conditions

[68] The numerical problem is second order in $x$ and first order in $t$, so that one initial and two boundary conditions are required for solution (Parker, e-book, 2004).

[69] The initial condition is expressed in terms of longitudinal profiles of elevation and grain size distributions of the surface layer and substrate. The initial bed elevation is computed as a linear function of an assumed initial channel slope $S|_{t=0}$ and downstream elevation $\eta_d|_{t=0}$:

$$\eta|_{t=0} = \eta_d|_{t=0} + \left(x - \frac{L}{2}\right) S|_{t=0}\,, \tag{18}$$

where $L$ is the length of the reach. Here $S|_{t=0}$, $\eta_d|_{t=0}$, and $L$ are user-specified parameters.

[70] The initial grain size distributions of the bed surface (i.e., active layer for the model) and of the substrate are also user-specified parameters. Here the former is assumed to be constant in the downstream direction, and the latter is considered constant both in the downstream and in the vertical directions. These initial conditions can be easily modified if the initial vertical stratigraphy of the deposit (substrate) and the downstream variation of the grain size distributions of the bed surface and substrate are known.

[71] The upstream boundary condition is specified in terms of the mean annual bed load input rate and the associated grain size distribution. In the model, these parameters

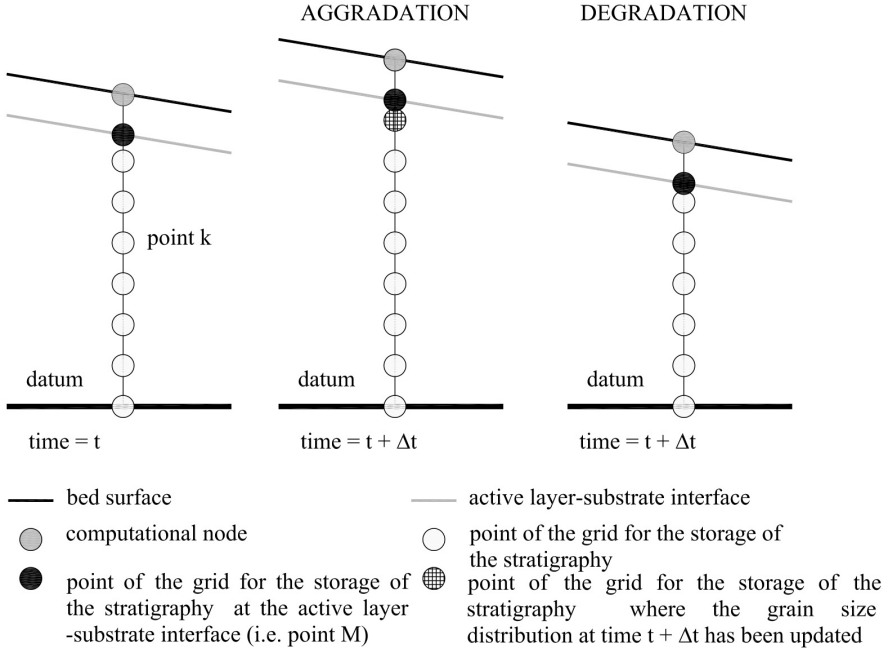


**Figure 8.** Grid to store and access the stratigraphy.

can, in principle, vary from year to year, but they must be the same within any annual hydrograph. In the present implementation, however, (1) the annual hydrograph is a specified parameter that does not vary downstream, and (2) mean annual input rate of channel bed sediment and the associated grain size distribution are taken to be constant throughout the run.

[72] The downstream boundary condition is expressed in terms of a fixed bed elevation at the downstream node. This condition should be placed, e.g., at a point with bedrock exposure. When such a fixed point is not available and the flow is assumed to be normal (steady and uniform), the downstream boundary condition can be placed (1) sufficiently far downstream so as not to affect the computations over the time span of interest or (2) at a confluence with a much larger river (Parker, e-book, 2004). In the numerical runs described in section 4, the downstream boundary condition was always placed sufficiently far downstream so as not to influence the results in the modeled domain.

## 4. Numerical Results

[73] As mentioned briefly in section 1, four groups of numerical runs were performed.

[74] 1. Zeroing runs were performed to calibrate the parameters of the model that cannot be estimated from the available data and to verify whether the model can reasonably reproduce conditions of mobile bed equilibrium inferred to be representative of the unregulated Trinity River. In particular, these runs were performed to adjust the value of the reference Shields number, equation (12), and to define the value of the parameter $a_{\text{trans}}$ in equation (17) in order to reach a dynamic equilibrium with a slope and a substrate similar to the predam Trinity River, under the assumption that the Trinity River was in equilibrium when the dams were built. The initial slope of the modeled domain was set equal to 0.002 m m$^{-1}$ in all the runs; the model was found to equilibrate at different slopes depending on the input rate of channel bed sediment and on the reference Shields number.

[75] 2. Test runs were performed to analyze the behavior of the model under different conditions and to compare the results with previous studies [e.g., *Parker et al.*, 2008]. In particular, these runs focused on exploring model results when (1) the feed rate is different from the estimated field value, (2) the procedure to store and access the stratigraphy is implemented, and (3) a constant bankfull width of the cross section is assumed.

[76] 3. Postdam runs were performed to determine whether the model can be reasonably applied to describe channel response at engineering time scales. To do this, the model was run with input parameters representative of the regulated Trinity River from 1962 (closure of the dams) to 2004.

[77] 4. Augmentation runs were performed to investigate the combined effect of regulated flood flow release and gravel augmentation on the regulated Trinity River.

[78] In the first two groups of runs the modeled domain extends from the confluence with Deadwood Creek to the confluence with Grass Valley Creek (see Figure 2). These runs refer to dynamic equilibrium that the flow and the sediment transport reach downstream of the hydrograph boundary layer [*Parker et al.*, 2008; *Wong and Parker*, 2006]. The simulations thus lasted for very long times (i.e., from 1800 to 15,000 years). The final results did not depend on the initial conditions because the river was modeled as a sediment feed flume [*Parker and Wilcock*, 1993]. In the last two sets of runs, however, the modeled domain is divided into two river segments (i.e., Lewiston and Bucktail/Lowden) because the input of sediment from the tributaries cannot be neglected. These runs refer to nonequilibrium conditions; the results are influenced by initial conditions because they describe the short term evolution of the river associated with an imposed change in the upstream boundary conditions.

### 4.1. Zeroing Runs

[79] The modeled reach of interest is approximately 11.5 km long. The number of computational nodes is 15, for a computational domain of 21 km. The length of the computational domain was set in order to have the downstream boundary condition far enough downstream of the reach of interest so as not to influence the dynamic equilibrium, and also to allow neglect of the first 4.5 km (three computational nodes) of the domain where the dynamic equilibrium is influenced by the upstream boundary conditions (i.e., the hydrograph boundary layer). In all the zeroing runs, the model was implemented so as to store and access the stratigraphy of the bed deposit.

[80] Results are reported in Table 1 and in Figures 9 and 10. All the output parameters presented in Table 1 and Figures 9 and 10 refer to the 11.5 km reach of interest, i.e., downstream of the hydrograph boundary layer and well upstream of the downstream boundary condition. In Table 1 the reference Shields number in the load relation $\tau^*_{ssrg}$, the value of $a_{\text{trans}}$, the sediment feed rate $Q_{\text{feed}}$, the length of the hydrograph boundary layer $L_{\text{hbl}}$, and the bed slope at equilibrium $S$ are reported for each run. The characteristic diameters of the bed surface at equilibrium (i.e., $D_{sg}$, $D_{s}50$, and $D_{s}90$) are also presented in Table 1. Finally, in Figure 9 the criterion to estimate the length of the hydrograph boundary layer is shown, and in Figure 10 the grain size distribution of the new substrate, averaged over the thickness of the new deposit and the length of the modeled domain, is plotted.

[81] In all the runs, the surface predicted by the model at mobile bed equilibrium is noticeably coarser than the substrate but not unrealistically so: the predicted values of $D_{sg}$

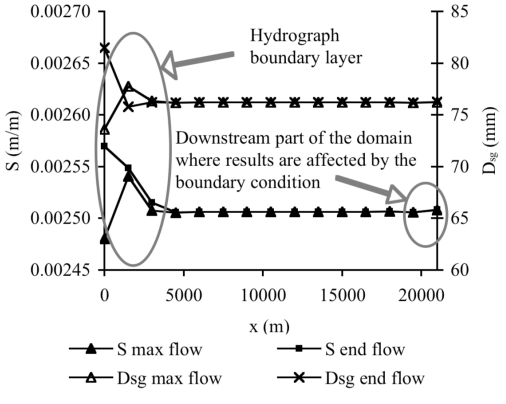


**Figure 9.** Plot illustrating the nature of the hydrograph boundary layer for run Z4. Here "max" refers to the maximum flow of the hydrograph, and "end" refers to the end flow (equal to low flow here) of the hydrograph.

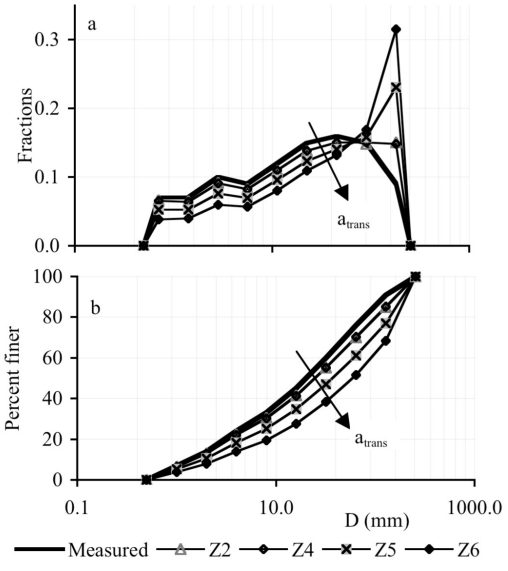


**Figure 10.** (a) Grain size fractions and (b) cumulative distributions of the substrate averaged over the thickness of the new deposit and over the length of the modeled domain in the zeroing runs.

and $D_{s50}$ are very close to the $D_{80}$ (77 mm) and the $D_{90}$ (122 mm) of the substrate, respectively. This indicates that at mobile bed equilibrium most of the finer sediment has been removed from the surface layer, leaving a coarser pavement to regulate the transport of all size ranges [*Parker et al.*, 1982; *Parker and Klingeman*, 1982].

[82] The length of the hydrograph boundary layer $L_{hbl}$ was defined by comparing values of bed slope and geometric mean size $D_{sg}$ in all the computational nodes at the maximum flow of the last hydrograph of the run and the low flow corresponding to the end of that hydrograph, as shown in Figure 9 for run Z4. It is assumed that the hydrograph boundary layer ends at the computational node where these values do not significantly change with the flow discharge. This means that the actual length of this region may be shorter than that reported in Table 1.

[83] The calibration of the model parameters can be summarized as follows.

[84] 1. As reported by *Gaeuman et al.* [2009], the bed load relation of *Wilcock and Crowe* [2003] reasonably predicts bed load transport rates on the Trinity River, but it requires some calibration to be properly implemented in a numerical model that describes the transport of nonuniform sediment at field scale. In the zeroing runs, this calibration is done in terms of $\tau^*_{ssrg}$, computed with equation (12) in runs Z1 and Z3 but computed by multiplying the value given by equation (12) by 0.5 in runs Z2 and Z4. The channel slope at mobile bed equilibrium is found to be similar to the present slope of the Trinity River in runs Z2 and Z4. Assuming that after the closure of the dams the released discharge was too low to cause significant changes to the longitudinal profile [*Gaeuman*, 2008b], the current slope of the Trinity River below Lewiston dam should not be significantly different from the predam slope (i.e., 0.0024 m m$^{-1}$). Thus the reference Shields number used here to apply the model to the Trinity River was computed by multiplying the value from equation (12) by 0.5 in order to bring the computed bed slope into agreement with the observed value. The consequences of lowering the reference Shields number in the bed load relation on the grain size distributions of the bed surface and of the substrate were also explored. In particular, comparing the results of the runs characterized by the same bed load feed rate, i.e., Z1 and Z2 and Z3 and Z4, it was found that (1) the value of the reference Shields number does not affect the grain size distribution of the substrate (Figure 10) and (2) the grain size distribution of the bed surface becomes coarser as the reference Shields number increases (see the characteristic diameters reported in Table 1).

[85] 2. The value of the parameter $a_{trans}$ that governs the grain size distribution of the sediment transferred to the substrate during bed aggradation, equation (17), is set equal to 0.2 in runs Z1–Z4, according to the results of the laboratory experiments of *Toro-Escobar et al.* [1996], who found 0.3, and *Viparelli et al.* [2010], who obtained 0.2. As shown in Figures 10a and 10b, the model reasonably reproduces the grain size distribution of the bed surface, even if it tends to overestimate the fraction of coarse sediment. In runs Z5 and Z6, $a_{trans}$ is set equal to 0.4 and 0.6, respectively, resulting in a computed substrate that is noticeably coarser than that measured in the field (Figures 10a and 10b). This is because the fraction of coarse sediment transferred from the active layer to the substrate increases with increasing $a_{trans}$. The grain size distribution of the bed surface does not depend on the value of $a_{trans}$, i.e., the characteristic diameters of the bed surface do not change from runs Z4 to Z5 and Z6 (Table 1). In all subsequent numerical runs presented in this paper, the parameter $a_{trans}$ is set equal to 0.2.

[86] Channel slopes and characteristic diameters of the bed surface at equilibrium vary with the sediment feed rate. More specifically, the equilibrium slope steepens and the bed surface becomes finer as the feed rate increases (compare runs Z1–Z3 and Z2–Z4). The effects of the sediment feed rate on the grain size distribution of the bed surface are discussed in more detail in section 4.2.

### 4.2. Test Runs

[87] The length of the modeled domain, the initial conditions, the input hydrograph, and the grain size distribution of the bed load input rate are the same as those of the zeroing runs.

[88] The test runs are summarized in Table 2, and the bed load input rates are also reported. In runs T1–T4 and

**Table 2.** Description of the Test Runs

| Run | $Q_b$ (t yr$^{-1}$) | Stratigraphy | $B$ |
|---|---|---|---|
| T1 | 1,000 | stored | equation (6) |
| T2 | 300,000 | stored | equation (6) |
| T3 | 3,000,000 | stored | equation (6) |
| T4 | 30,000,000 | stored | equation (6) |
| T5 | 1,000 | not stored | equation (6) |
| T6 | 16,199 | not stored | equation (6) |
| T7 | 31,850 | not stored | equation (6) |
| T8 | 300,000 | not stored | equation (6) |
| T9 | 3,000,000 | not stored | equation (6) |
| T10 | 30,000,000 | not stored | equation (6) |
| T11 | 16,199 | stored | const = 84 m |
| T12 | 31,850 | stored | const = 84 m |

T11–T12, the model is allowed to store and access the stratigraphy of newly deposited sediment ("stored" in the stratigraphy column), while in runs T5–T10, the grain size distribution of the substrate was assumed to be constant in time and space and equal to the distribution represented in Figure 4 ("not stored" in the stratigraphy column). Finally, in runs T1–T10 the channel width is assumed to vary with the flow discharge according to equation (6) and Figure 7, while in the last two runs (T11 and T12) the width of the cross section is constant and equal to its predam reference value (i.e., 84 m).

[89] The motivation for the runs with and without the storage of stratigraphy merits clarification. *Parker et al.* [2008] present a similar calculation of the morphodynamic response of a gravel bed river to an imposed hydrograph. In their Figure 10.19, pertaining to mobile bed equilibrium, however, it is seen that the geometric mean of the bed load size distribution averaged over the hydrograph at the downstream end of the domain nearly, but not precisely, satisfies the necessary condition that it must be equal to that of the feed. This discrepancy is a result of the absence of a means to store and access stratigraphy in that model. The present model corrects this deficiency of that earlier model.

[90] In Figure 11, $D_{sg}$ and the geometric mean diameter of the bed load $D_{lg}$ at the maximum flow and the low end flow of the last hydrograph at the downstream node of the domain are plotted as functions of the bed load input rate (corresponding to runs T1, Z2, Z4, T2, T3, and T4 in order of increasing feed rate). The geometric mean diameter of the bed load input rate ($D_{lg\ \mathrm{feed}}$) and of the bed load transport rate averaged over the last hydrograph ($D_{lg\ \mathrm{av}}$) are also shown in Figure 11. To interpret the results, two limiting cases need to be defined: static armor and unarmored bed [*Parker et al.*, 2008]. Static armor is approached as the feed rate becomes increasingly smaller, with the fine grains essentially washed out from the bed surface so as to leave an immobile, coarse bed surface. When the transport rate becomes increasingly high, on the other hand, the bed surface tends to become unarmored and have the same grain size distribution as the feed (and thus of the substrate if the feed and substrate have the same grain size distribution).

[91] A comparison illustrating the extent of the hydrograph boundary layer $L_{\mathrm{hbl}}$, the bed slope, and the grain size distribution of the bed surface averaged over the length of the modeled domain at equilibrium for the zeroing runs Z2 and Z4 and for the test runs T1–T4 is presented in Table 3 and in Figures 11, 12, and 13.

[92] The results of this second group of numerical runs show that the following results occur as the bed load feed rate increases.

[93] 1. The hydrograph boundary layer becomes longer, and, indeed, in runs T3 and T4 it is longer than the modeled domain (Figure 12). Therefore, bed slopes, geometric mean diameters, and grain size distributions of the surface layer reported in Table 3 and Figures 11 and 12 refer to (1) the reach outside of the boundary layer for runs Z2, Z4, T1, and T2 and (2) the downstream 12 computational nodes for runs T3 and T4 (i.e., the part of the domain where the channel slope does not vary too much during the hydrograph).

[94] 2. The geometric mean diameters of the feed and of the bed load averaged over the last hydrograph are nearly equal for all the runs shown in Figure 11.

[95] 3. Geometric mean diameters of the bed surface at high flow and at the end of the last hydrograph are

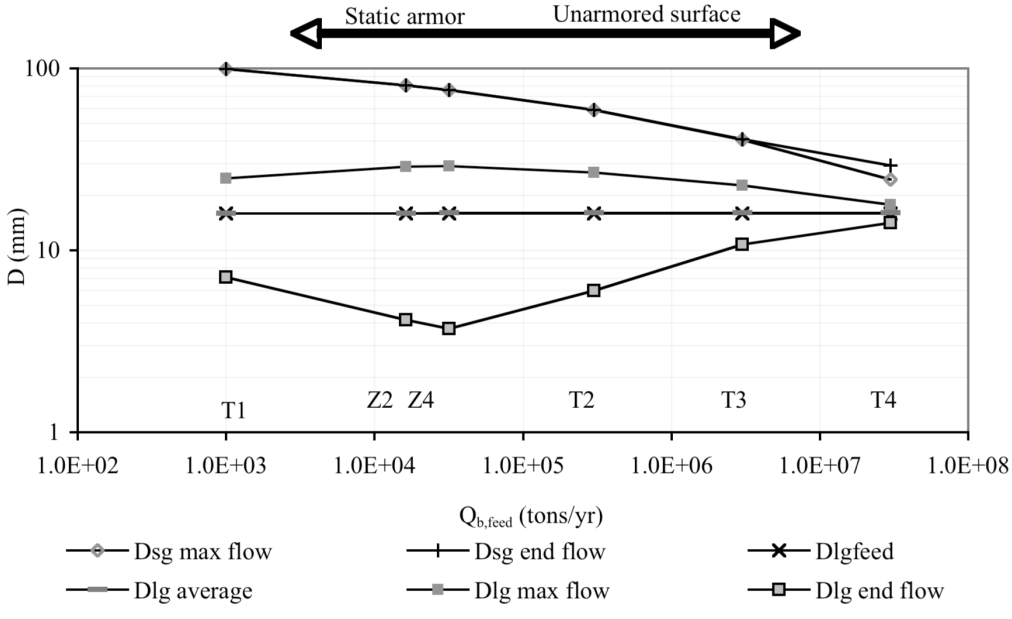


**Figure 11.** Variation during the last hydrograph of (1) the geometric mean diameter of the bed surface at the last computational node of the domain at the maximum flow ($D_{sg\ \mathrm{max\ flow}}$) and at the low-flow end of the run ($D_{sg\ \mathrm{end\ flow}}$), (2) the geometric mean diameter of the feed ($D_{sg\ \mathrm{feed}}$), and (3) the geometric mean diameter of the load at the last computational node of the domain averaged over the hydrograph ($D_{lg\ \mathrm{average}}$), at maximum flow ($D_{lg\ \mathrm{max\ flow}}$), and at the low flow at the end of the run ($D_{lg\ \mathrm{end\ flow}}$).

**Table 3.** Length of the Hydrograph Boundary Layer $L_{hbl}$, the Bed Slope at Maximum Flow $S_{max\ flow}$ and at the end $S_{end\ flow}$ of the Last Hydrograph, and the Reach-Averaged Geometric Mean Diameter of the Bed Surface at the End of the Last Hydrograph $D_{sg\ end\ flow}$ for Zeroing Runs Z2 and Z4 and for Test Runs T1–T4

| Run | $Q_b$ (t yr$^{-1}$) | $L_{hbl}$ (m) | $S_{max\ flow}$ (m m$^{-1}$) | $S_{end\ flow}$ (m m$^{-1}$) | $D_{sg\ end\ flow}$ (mmol) |
|---|---|---|---|---|---|
| T1 | 1,000 | 3,000 | 0.0016 | 0.0016 | 99 |
| Z2 | 16,199 | 4,500 | 0.0023 | 0.0023 | 81 |
| Z4 | 31,850 | 4,500 | 0.0025 | 0.0025 | 76 |
| T2 | 300,000 | 13,500 | 0.0039 | 0.0039 | 59 |
| T3 | 3,000,000 | ≥21,000 | 0.0077 | 0.0079 | 40 |
| T4 | 30,000,000 | >21,000 | 0.0264 | 0.0263 | 25 |

noticeably different for run T4 only, for which the hydrograph boundary layer is much longer than the modeled domain (Figure 11).

[96] 4. The bed load transport rate at high flow is always coarser than that corresponding to low flow (Figure 11).

[97] 5. As the feed rate increases, unarmored conditions are approached (Figure 11). The bed surface becomes more and more similar to the feed rate (and the substrate), and the difference between the grain size distributions of the bed load at high and low flow decreases. As the feed rate becomes progressively smaller and conditions of static armor are approached, the opposite behavior is observed. That is, progressing in order from run Z4 to Z2 to T1, the predicted grain size distributions of the bed load at high and low flow tend to become similar to the grain size distribution of the feed. This inconsistency was also observed by *Parker et al.* [2008], and it probably depends on the sediment transport equation implemented in the code, which has not been derived so as to represent such low transport conditions.

[98] 6. The channel becomes steeper and its surface becomes finer (Table 3 and Figures 11 and 13). In particular, as the bed load input rate (equal to the sediment transport rate averaged over the last hydrograph for all the runs) increases, the geometric mean diameter of the bed surface tends to become equal to the geometric mean diameter of the sediment feed rate.

[99] The results of runs T3 and T4 for the last hydrograph of each run illustrate the changes in channel slope and grain size distribution in the hydrograph boundary layer (Figure 12).

[100] 1. The grain size distribution of the bed surface becomes finer as the water discharge increases, and it then coarsens when the flow decreases and is no longer able to transport the coarser fractions.

[101] 2. The channel slope strongly varies with the water discharge in the first three computational nodes (i.e., 3000 m) and then remains more or less constant over the downstream part of the domain. In particular, in the first three nodes the slope at high flow is milder than the slope at low flow. This is because the sediment is fed at a constant rate; at higher discharges the flow locally erodes part of the bed, but deposition occurs as discharges progressively decrease on the falling limb of the hydrograph.

[102] Figure 14, which has the same format as Figure 11, shows a comparison between runs with and without the

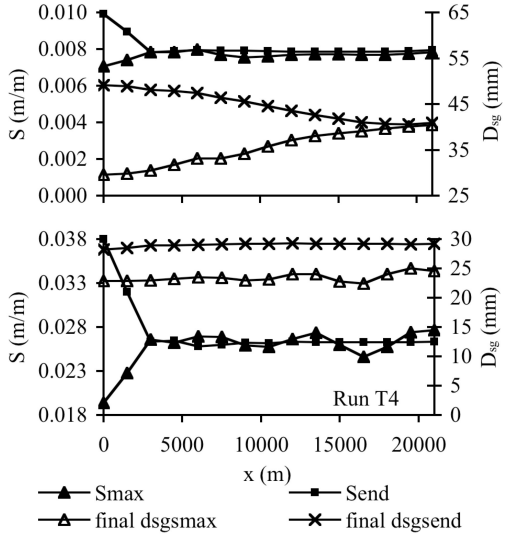


**Figure 12.** Variation in the downstream direction of channel slope $S$ and geometric mean diameter of the bed surface $D_{sg}$ at high (max) and low flow (end) during the last hydrograph for runs T3 and T4.

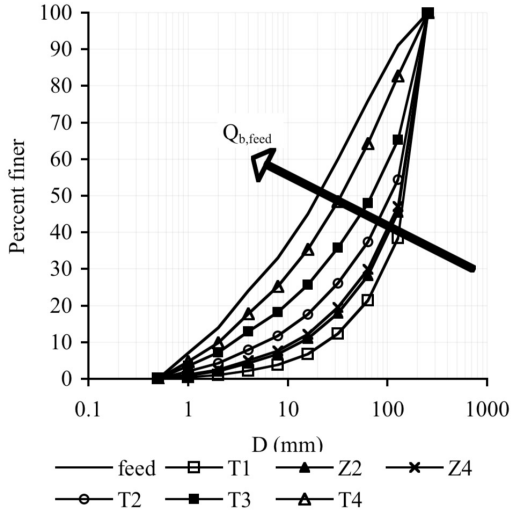


**Figure 13.** Grain size distributions of the bed surface averaged over the channel length downstream of the boundary layer in the zeroing runs Z2 and Z4 and in the test runs T1–T4. Also shown is the grain size distribution of the sediment feed.

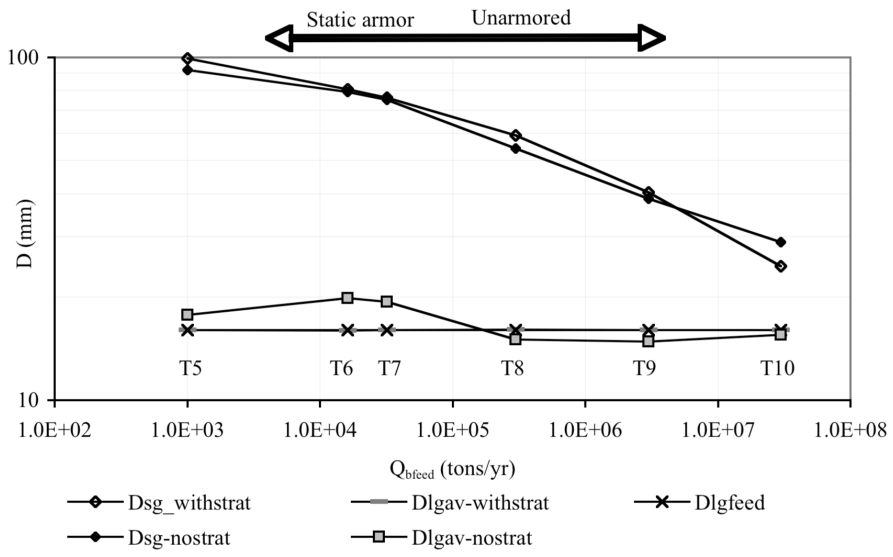


**Figure 14.** Comparison between the geometric mean diameter of the bed surface and of the bed load averaged over the last hydrograph for the runs, as computed with and without storage of the stratigraphy ($D_{sg\_withstrat}$, $D_{sg\text{-}nostrat}$, $D_{lgav\_withstrat}$, and $D_{lg\text{-}nostrat}$, respectively).

storage of the stratigraphy. The values of $D_{sg}$ at the last computational node at the end of the runs and the values of $D_{lg}$ in the same computational node averaged over the last hydrograph are plotted as functions of the sediment feed rate for runs T1–T4, Z2, Z4, and T5–T10. In Figure 14, $D_{sg\text{-}withstrat}$ and $D_{lgav\text{-}withstrat}$ refer to values of $D_{sg}$ and $D_{lg}$ computed with the storage of stratigraphy implemented, and $D_{sg\text{-}nostrat}$ and $D_{lgav\text{-}nostrat}$ refer to the corresponding values with no stratigraphic storage implemented. In this latter case, the substrate is always assumed to have the same grain size distribution, regardless of the history of aggradation and degradation. Also shown in Figure 14 is $D_{lgfeed}$. Even in the runs with no storage of stratigraphy, the bed surface always becomes progressively finer as the sediment feed rate increases. At mobile bed equilibrium, the parameter $D_{lgav}$ must be precisely equal to $D_{lgfeed}$. Figure 14 demonstrates that this condition is not satisfied in the absence of storage stratigraphy (as in the model of *Parker et al.* [2008]) but is satisfied in the present model.

[103] In the last two runs in Table 2, T11 and T12, the channel width is assumed to be constant and equal to its predam bankfull value, and the input parameters are those of runs Z2 and Z4, respectively. In runs T11 and T12 and Z2 and Z4 the length of the boundary layer is practically the same (i.e., 4500 m). The bed slopes are milder in run T11 as compared to run Z2 (with respective values of 0.0022 and 0.0024). The same trend was observed in run T12 as compared to run Z4 (with respective slopes of 0.0023 and 0.0025). The corresponding bed surfaces are finer (with values of 79 versus 81 mm in runs T11 and Z2, respectively, and 75 versus 76 mm in runs T12 and Z4, respectively). These results can be explained considering that in the runs with constant width (T11 and T12) the water discharge and the sediment feed rate per unit channel width at high flow are higher than in the runs with variable width (Z2 and Z4). This results in a milder slope because of the increase in water discharge per unit width and in a finer bed surface for the higher sediment feed rate per unit width associated with high flows when conditions of constant width are imposed.

### 4.3. Postdam Run

[104] The modeled stretch of the Trinity River is divided in two segments: the Lewiston segment from the confluence with Deadwood Creek to the confluence with Rush Creek and the Bucktail/Lowden segment from the confluence with Rush Creek to the confluence with Grass Valley Creek. The Lewiston segment is approximately 5 km long, and the length of the modeled domain is equal to 9 km (in order to place the downstream boundary condition sufficiently far downstream so as not to influence the results of the simulations in the reach of interest). The modeled domain is divided in 13 segments bounded by 14 computational nodes. The Bucktail/Lowden segment is 7 km long, and the length of the numerical domain is set equal to 12 km, divided in 13 segments bounded by 14 computational nodes.

[105] The input hydrograph is reported in Figure 3. The sediment feed rates are 3861 and 5425 t $yr^{-1}$ for the Lewiston and the Bucktail/Lowden segments, respectively, and their size distributions are plotted in Figure 6b. The downstream boundary condition (i.e., constant bed elevation) is again placed farther downstream so as not to influence the results in the domain of interest.

[106] For each segment, three numerical runs, PD1, PD2, and PD3, were performed, as summarized in Table 4. Each run actually consists of a pair of runs, i.e., one for the Lewiston segment and one for the Bucktail/Lowden segment. It has been necessary to run more than one numerical simulation for each segment. This is because (1) the predam grain size distribution of the bed surface is unknown and (2) for runs PD1 and PD2, which were of the short duration of 42 years, the results at the end of the computations depend on the initial conditions in that they refer to conditions of nonequilibrium.

**Table 4.** Description of the Postdam Runs

| Run | Surface Size Distribution | Lewiston Segment | | | Bucktail/Lowden Segment | | |
|---|---|---|---|---|---|---|---|
| | | $Q_{b\ \text{feed}}$ (t yr$^{-1}$) | $D_{lg\ \text{feed}}$ (mmol) | Duration (years) | $Q_{b\ \text{feed}}$ (t yr$^{-1}$) | $D_{lg\ \text{feed}}$ (mmol) | Duration (years) |
| PD1 | substrate | 1352 | 45 | 42 | 2003 | 22 | 42 |
| PD2 | Z4 | 1352 | 45 | 42 | 2003 | 22 | 42 |
| PD3 | Z4 | 1352 | 45 | 66,000 | 2003 | 22 | 96,000 |

[107] Runs PD1 and PD2, although spanning the same period (from 1962 to 2004), differ in the initial grain size distribution of the bed surface. In run PD1, the initial bed has the same grain size distribution as the substrate, while in run PD2 it has the same grain size distribution as that of the bed surface computed at mobile bed equilibrium for run Z4. The values of $D_{s50}$ and $D_{s90}$ computed at mobile bed equilibrium (i.e., 125 and 223 mm, respectively, in both segments) are greater than the reach-averaged field values but smaller than the maximum recorded values (i.e., 190 and 380 mm). The initial condition for run PD1 is unrealistic because it means that the predam Trinity River did not show any armoring of the bed surface, which corresponds to a feed rate that is 3 or 4 orders of magnitude higher than our estimate (Figure 11). On the other hand, it represents the finest possible grain size distribution of the bed surface.

[108] The different initial grain size distributions of the bed surface of runs PD1 and PD2 result in opposite behavior for the 42 year simulation of regulated period.

[109] 1. The bed surface becomes coarser during run PD1: at the end of the run, $D_{s50}$ and $D_{s90}$ are approximately equal to 85 and 202 mm, respectively, for both segments. These values are very close to the reach-averaged field values (i.e., $D_{s50} = 90$ mm and $D_{s90} = 198$ mm). On the other hand, at the end of run PD2, $D_{sg}$ decreases in the two segments (from 76 to 59 mm in the Lewiston segment and to 55 mm in the Bucktail/Lowden segment). This decrease is specifically associated with an increase in the sand and very fine gravel content in the surface.

[110] 2. The bed slope slightly decreased from 0.0024 m m$^{-1}$ to approximately 0.0022 m m$^{-1}$ in both segments during run PD1, while it did not change during run PD2.

[111] Run PD3 describes the mobile bed equilibrium for the postdam boundary conditions. The results outside the hydrograph boundary layer are independent of the initial conditions. The length of the hydrograph boundary layer was found to be approximately 2000 m for the Lewiston segment and 2500 m for the Bucktail/Lowden segment.

[112] The bed surface at mobile bed equilibrium for run P3 is finer than for the predam run Z4, as shown in Figure 15, because the fractions of sediment in the coarsest size ranges in the feed rate are smaller than those of the initial substrate. The bed slope at the end of run PD3 is 0.00097 m m$^{-1}$ for the Lewiston segment and 0.00092 m m$^{-1}$ for the Bucktail/Lowden segment because of the greatly reduced flow discharge as compared to predam conditions. Note that the duration of time necessary to achieve mobile bed equilibrium, i.e., 66,000 and 96,000 years for the Lewiston and the Bucktail/Lowden segment, respectively, is unrealistically long. The results of the run nevertheless give an idea of the direction in which the channel would evolve were postdam conditions continued indefinitely.

[113] As underlined above, the result of the runs PD1 and PD2 strongly depend on the initial conditions because they refer to a very short time scale, so that channel morphodynamics and sediment transport do not have time to equilibrate (see duration columns in Table 4). Moreover, the input hydrograph has been derived from the flow duration curve based on the discharges measured at the USGS gauging station at Lewiston and thus is not entirely representative of the flow regime in the modeled domain. It does not consider, for example, that in the first decade after the closure of the dams, flow releases were very small (4−8 m$^3$ s$^{-1}$) and that they changed irregularly in the following years [*U.S. Fish and Wildlife Service and Hoopa Valley Tribe*, 1999]. Finally, the bed load input rate is assumed to be constant over the hydrograph and the historical gravel augmentations are not properly modeled.

[114] These limitations notwithstanding, an important result deserves mention. The model predicts an increase in the content of sediment finer than 6 mm in the surface layer in runs PD2 (13%−15% from an initial 6.5%) and also in the fraction of sand in the surface layer (7%−9% from an initial 2.5%). At equilibrium (run PD3) the fraction of sediment in the surface layer finer than 6 mm varies between

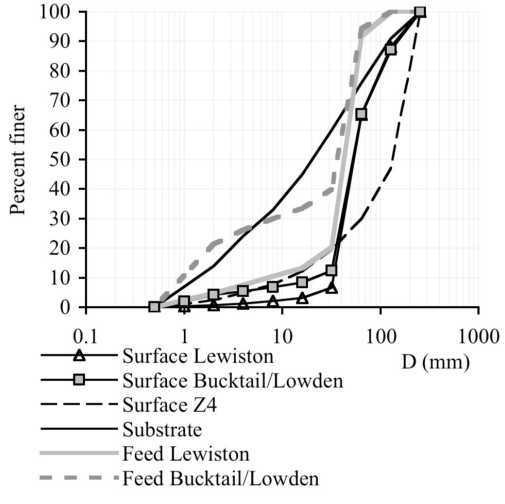


**Figure 15.** Grain size distributions of the bed surface averaged over the channel length (but outside the hydrograph boundary layer) at the end of run PD3. For the Lewiston segment, $D_{sg}$ is 30 mm, $D_{s50}$ is 50 mm, $D_{s90}$ is 127 mm, the fraction of sediment finer than 6 mm is 21%, and the fraction of sand in the bed surface is 12.5%. For the Bucktail/Lowden segment, $D_{sg}$ is 25 mm, $D_{s50}$ is 51 mm, $D_{s90}$ is 114 mm, the fraction of sediment finer than 6 mm is 25%, and the fraction of sand in the bed surface is 15.4%.

21% and 25%, and the corresponding fraction of sand varies between 12% and 16%. These results are in good agreement with the reduction of gravel quality due to the infiltration of fine sediment reported by *Graham Matthews and Associates* [2001] and also with the visual estimate of an approximate reach-averaged content of sand in the surface layer of 10% based on the mapping of 2006 and 2007.

[115] To confirm the ability of the model to reproduce the infiltration of fine sediment in the substrate of the Trinity River in the regulated period, the grain size distributions of the topmost layer of the substrate at the end of runs PD2 and PD3 are plotted in Figure 16 along with the grain size distributions of the feed rate and initial substrate. During the 42 years of simulation of the run PD2, the model predicts an increase in sediment finer than 6 mm in the modeled domain from 29% to 36% in the Lewiston segment and to 39% in the Bucktail/Lowden segment. *Kondolf* [2000] reports numerous research results on the fraction of material finer than 6 mm beyond which less than 50% emergence of salmonids is realized. In Kondolf's Table 1, this fraction is seen to range from 15% to 40%, depending upon the study in question, with an average value of 30%. With this in mind, the predictions of the model of 36% for the Lewiston segment and 39% for the Bucktail/Lowden segment are verging toward values that are too high for a healthy spawning environment.

[116] When the flow and the sediment transport reach equilibrium (runs PD3), the grain size distribution of the substrate is very close to the grain size distribution of the bed load feed rate, and the fraction of sediment finer than 6 mm in the substrate is 68% in the Lewiston segment and 72% in the Bucktail/Lowden segment. These results highlight the tendency of postrun conditions to promote an unhealthy environment for salmonid spawning. The small difference between the grain size distribution of the bed load and the topmost layer of the substrate at the end of run PD3 that is apparent in Figure 16 corresponds to the loss of information due to the averaging process in the vertical direction associated with the procedure to store and access stratigraphy.

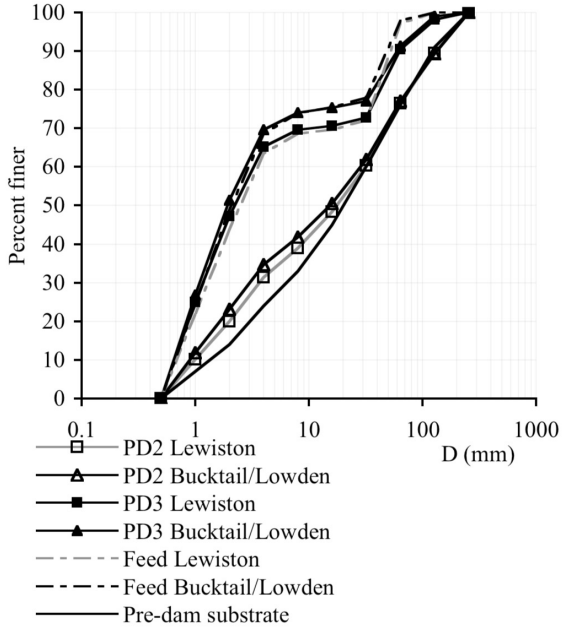


**Figure 16.** Comparison between the grain size distributions of the topmost layer of the substrate in runs PD2 and PD3 for the Lewiston and the Bucktail/Lowden segments, the sediment feed rate, and the predam substrate.

### 4.4. Augmentation Runs

[117] Four groups of runs were performed to investigate the consequences that the gravel augmentations proposed by *Gaeuman* [2008b] may have in the upstream part of the regulated Trinity River, i.e., runs AU1–AU4 in Table 5. These augmentations are characterized by two possible feed rates each (i.e., 9091 and 13,636 t $yr^{-1}$) for the two different grain size distributions represented in Figure 17. The bed load input rates and their grain size distributions have been computed by adding the augmentation values to the postdam bed load input values for the Lewiston and Bucktail/Lowden segments, under the assumption that the gravel associated with augmentation is introduced in the Lewiston segment. The grain size distributions of the bed load input are shown in Figure 17 for the two modeled segments; the bed load input rates are reported in Table 5 along with other input parameters (i.e., augmentation feed rate, type of added gravel, and geometric mean diameter of the bed load input rate). The input hydrograph, reported in Figure 3, has been computed from the mandated ROD flow releases.

[118] The results of the augmentation runs strongly depend on the initial conditions because they describe the changes in the regulated Trinity River for an engineering time scale of 120 years, i.e., much shorter than the geological time scale required for the flow and the sediment transport to reach equilibrium. The initial river bed is the same as that assumed in the postdam runs (i.e., bed slope of 0.0024 m $m^{-1}$ and substrate with the grain size distribution represented in Figure 4) and thus provides a reasonable approximation of the present conditions of the river. The initial grain size distribution of the bed surface (Figure 17) has been determined using the available field data ($D_{s50}$ = 90 mm, $D_{s90}$ = 198 mm, and 10% sand).

[119] The results of the augmentation runs are reported in Table 6 and Figure 18. In Table 6, for each modeled segment the channel slope $S$, the reach-averaged fraction of sand in the surface layer $F_{ssurf}$ and $D_{s50}$ and $D_{s90}$ are presented along with $D_{lgav}$. In Figure 18 the grain size distributions of the topmost layer of the substrate are compared with the predam substrate.

[120] During the augmentation runs, the following occur.

[121] 1. Noticeable channel bed aggradation (i.e., an increase in bed slope from 0.0023 to 0.0027) is evident for run AU4, for which the coarse gravel is added at the higher rate. In runs AU2 and AU3 the bed profile does not change significantly in the two segments. The aggradation predicted in the Lewiston segment is, to some extent, a numerical artifact related to the quick change of grain size distribution of the bed surface as the fine sediment is rapidly washed out. This results in a rapid increase in roughness height computed with equation (5), causing some bed steepening. As time passes and the flow and the sediment

**Table 5.** Description of the Augmentation Runs

| Run | Augmentation Rate (t yr$^{-1}$) | Augmentation Gravel | Lewiston Segment | | Bucktail/Lowden Segment | |
|---|---|---|---|---|---|---|
| | | | $Q_{b\ \mathrm{feed}}$ (t yr$^{-1}$) | $D_{lg\ \mathrm{feed}}$ (mmol) | $Q_{b\ \mathrm{feed}}$ (t yr$^{-1}$) | $D_{lg\ \mathrm{feed}}$ (mmol) |
| AU1 | 9,091 | fine | 11,873 | 15.5 | 13,437 | 12.3 |
| AU2 | 9,091 | coarse | 11,873 | 16.9 | 13,437 | 13.3 |
| AU3 | 13,636 | fine | 16,418 | 18.7 | 17,982 | 15.4 |
| AU4 | 13,636 | coarse | 16,418 | 20.5 | 17,982 | 16.8 |

transport tend to reach equilibrium, the bed slope tends to return toward the initial value.

[122] 2. The content of sand in the surface layer decreases, as shown in Table 6, and becomes smaller for the runs characterized by the coarser gravel feed rate. That is, this fraction decreases from an initial value of 10% to 2.2%−3.1% in the Lewiston segment and 3.5%−4.5% in the Bucktail/Lowden segment. The model thus indicates that gravel augmentation will help in removing fine sediment from the bed surface.

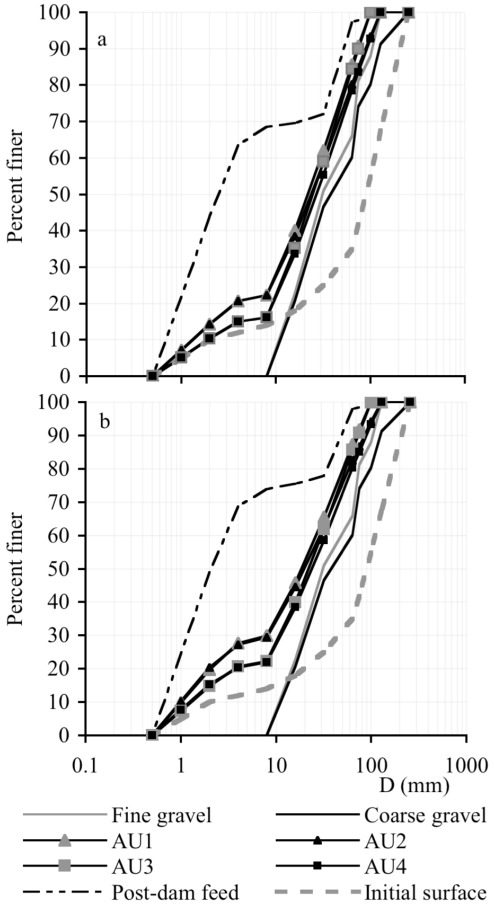


**Figure 17.** Grain size distributions of the augmented gravel (fine and coarse), of the postdam bed load feed rate, of the bed load input rates for the augmentation runs (AU1–AU4), and of the initial bed surface for (a) the Lewiston segment and (b) the Bucktail/Lowden segment.

[123] 3. The reach-averaged $D_{s50}$ becomes finer in all the runs, while the reach-averaged $D_{s90}$ becomes significantly finer only when the coarse gravel is added at the higher rate (i.e., run AU4).

[124] 4. The geometric mean diameter of the bed load averaged over the last hydrograph is not too different from the same diameter of the bed load input rate (as can be seen by comparing Tables 5 and 6) in all the runs and in both modeled segments, showing that after 120 years the sediment transport regime may not be too far from a condition of mobile bed equilibrium. Another piece of evidence indicating that the conditions at the end of these runs may be close to equilibrium is the similarity between the grain size distributions of the substrate represented in Figure 18 and the grain size distributions of the feed rate shown in Figure 17.

[125] Figure 18 indicates that the major difference between the present-day (postdam) grain size distribution of the substrate and those at the end of the augmentation runs is a marked decrease in the content of fine sediment after augmentation. The fraction of sediment finer than 6 mm decreases in the Lewiston reach from an initial value of 29% to 25% and 22% in runs AU1 and AU2, respectively, and to 17% and 16% in runs AU3 and AU4, respectively. All of these postaugmentation values are below the average threshold value of 30% of *Kondolf* [2000], beyond which less than 50% of salmonids emerge from redds. In the Bucktail/Lowden segment, the fraction of sediment finer than 6 mm does not change by the end of runs AU1 and AU2 but decreases to 25% and 21% for the higher augmentation rates of runs AU3 and AU4, respectively. Again, all these values are below the quoted threshold value of 30%. The median diameter of the substrate varies between 16 and 32 mm, which corresponds to a minimum length of the spawning fish of 200–300 mm [*Kondolf*, 2000], a value that is smaller than the characteristic length of the present-day salmonid population of the Trinity River [*Kondolf et al.*, 1993].

## 5. Conclusion

[126] In this paper, we describe a tool that is intended to help in the design of gravel augmentations in gravel bed rivers. The tool consists of a one-dimensional numerical model that predicts the conditions of mobile bed equilibrium in a gravel bed river under an imposed cycled hydrograph in terms of channel slope and grain size distributions of the bed surface and of the substrate. The tool is of similar structure to the model presented by *Parker et al.* [2008] to describe the morphodynamic evolution of a gravel bed river under an imposed cyclic hydrograph. The present model, however, stores and accesses the stratigraphy of the bed deposit and considers at-a-station variation of channel

**Table 6.** Results of the Augmentation Runs[a]

| | Lewiston Segment | | | | | Bucktail/Lowden Segment | | | | |
|---|---|---|---|---|---|---|---|---|---|---|
| Run | $S$ (m/m) | $F_{ssurf}$ | $D_{s50av}$ (mmol) | $D_{s90av}$ (mmol) | $D_{lgav}$ (mmol) | $S$ (m m$^{-1}$) | $F_{ssurf}$ | $D_{s50av}$ (mmol) | $D_{s90av}$ (mmol) | $D_{lgav}$ (mmol) |
| AU1 | 0.0023 | 3.1% | 74 | 207 | 15.6 | 0.0023 | 4.5% | 80 | 212 | 12.6 |
| AU2 | 0.0025 | 2.9% | 83 | 186 | 17.3 | 0.0024 | 4.4% | 88 | 200 | 13.7 |
| AU3 | 0.0025 | 2.6% | 65 | 186 | 18.5 | 0.0024 | 3.6% | 72 | 202 | 15.4 |
| AU4 | 0.0027 | 2.2% | 76 | 144 | 20.7 | 0.0025 | 3.5% | 78 | 170 | 17.1 |

[a]$S$ is the bed slope, $F_{ssurf}$ denotes the fraction of sand in the surface layer (10% in the initial surface), $D_{s50av}$ and $D_{s90av}$ represent the reach-averaged value of the median diameter and of the $D_{90}$ of the bed surface (90 and 198 mmol, respectively, in the initial surface), and $D_{lgav}$ is the geometric mean diameter of the load averaged over the last hydrograph.

width with flow discharge. The implementation of the procedure to store and access the stratigraphy ensures that at mobile bed equilibrium the grain size distribution of the bed load averaged over the hydrograph is everywhere identical to that of the feed. The earlier model of *Parker et al.* [2008] did not satisfy this condition.

[127] The tool is applied to predict the effects of gravel augmentations and mandated annual flow releases on the regulated Trinity River in California. The application of the model proceeded in four steps.

[128] 1. Zeroing runs were performed under the assumption that that river was in equilibrium just prior to the installation of the dams, allowing calibration of the parameters of the model in order to predict reasonable conditions of mobile bed equilibrium for the unregulated river.

[129] 2. Test runs were then performed to investigate the behavior of the model for different bed load input rates in a generic generalization of the Trinity River. The present results are in agreement with previous studies [e.g., *Parker et al.*, 2008; *Wong and Parker*, 2006; *Hassan et al.*, 2006]: as the sediment feed rate increases, the hydrograph boundary layer becomes longer, and the grain size distributions of the bed surface and of the bed load tend to become similar to the grain size distribution of the feed rate. In particular, as the sediment feed rate increases and the surface armor becomes finer, the grain size distributions of the load during the hydrograph become similar to the feed rate regardless of the magnitude of the discharges in the hydrograph. These two first steps were necessary to ensure that the model can reasonably predicts conditions of mobile bed equilibrium.

[130] 3. The next step consists of the validation of the model for a much shorter time scale and for conditions that are far from the equilibrium. In particular, the 42 years of regulated flow regime from 1962 (closure of the dams) to 2004 have been simulated. These runs show that the model is able to capture and reproduce the postdam increase in content of fine sediment in the gravel bed that is, among other reasons, responsible for the deterioration of the spawning gravel and of the aquatic habitat.

[131] 4. Finally, the model has been applied to investigate the effects of gravel augmentations on the upstream part of the regulated Trinity River. Four different augmentation plans have been considered, i.e., two different augmentation rates with two different grain size distributions. In all the runs, the model predicts an improvement of the quality of the spawning environment because the median diameter of the bed surface and the fraction of fine sediment in the topmost part of the bed deposit decrease so as to meet the requirements given by *Kondolf* [2000] for a healthy spawning environment. The numerical results also show that under the conditions of the mandated flow releases, the channel bed elevation and $D_{s90}$ significantly change only in the case of run AU4, corresponding to the highest of gravel augmentation and the coarsest grain size distribution. In particular, in the case of run AU4, the model predicts bed aggradation and a reduction of the $D_{s90}$ from 198 to 144 and 177 mm in the Lewiston and Bucktail/Lowden segments, respectively. This result can be interpreted as a sign that under the mandated flow releases, this particular augmentation plan may not be appropriate for the Trinity River because it would cause morphological changes that may not be appropriate for the present river system. For the other three augmentation plans, the tool does not predict any significant change in the bed profile.

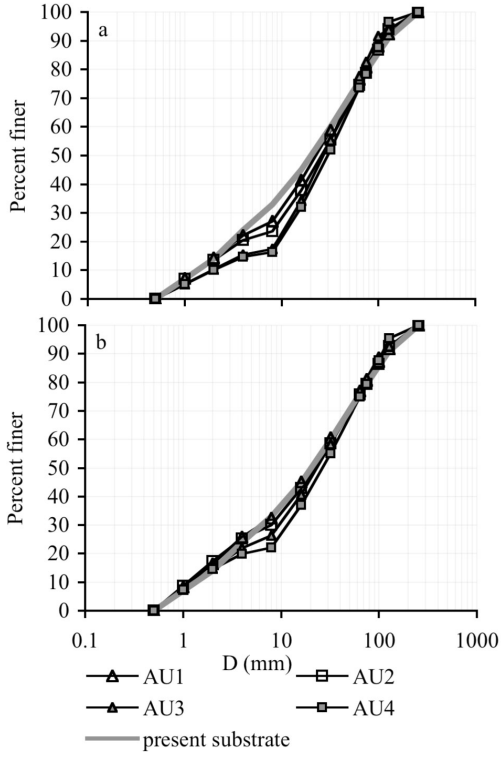


**Figure 18.** Grain size distributions of the topmost part of the substrate for the augmentation runs AU1–AU4 and of the postdam (but preaugmentation) substrate for (a) the Lewiston segment and (b) for the Bucktail/Lowden segment.

Moreover, after 120 years the geometric mean diameter of the bed load transport rate averaged over the last hydrograph is similar to the geometric mean diameter of the feed rate. This result confirms that if these augmentation plans are implemented, the river should reach conditions that are not too far from the mobile bed equilibrium in a relatively short period of time, and consequently, dramatic and unexpected changes in river morphology should not occur.

[132] The model used to perform the above calculations is embedded in an Excel spreadsheet called the Spawning Gravel Refresher, a stream restoration tool that is being made available to the engineering, scientific, and river restoration community through the Web site of the National Center for Earth-surface Dynamics. More specifically, the tool, which consists of an Excel workbook with embedded code in Visual Basic for Applications, is available in the National Center for Earth-surface Dynamics stream restoration toolbox.

## Notation

$a_{\text{trans}}$ parameter characterizing the material released to the substrate as the bed aggrades.
$a_u$ upwinding coefficient to compute the spatial derivatives.
$b$ exponent in the equation to compute the parameter $\phi_i$ in the load relation of *Wilcock and Crowe* [2003].
$B$ channel width.
$B_{\text{ref}}$ reference channel width.
$D_i$ characteristic diameter of the $i$th size range of the grain size distribution.
$D_{sg}$ geometric mean diameter of the bed surface.
$D_{s50}$ median diameter of the bed surface.
$D_{s90}$ diameter of the bed surface such that the 90% of the sediment is finer.
$f_{Ii}$ fraction of sediment in the $i$th size range exchanged between the active layer and the substrate as the river bed aggrades and degrades.
$F_i$ fraction of sediment of the bed surface in the $i$th size range.
$F_s$ fraction of sand in the bed surface.
$g$ acceleration of gravity.
$G(\phi_i)$ function to compute the grain size-specific bed load transport rate for the load relation of *Wilcock and Crowe* [2003].
$H$ water depth.
$k_s$ roughness height.
$L$ channel length.
$L_a$ active layer thickness.
$L_s$ thickness of the grid for the storage of the stratigraphy.
$M$ number of computational nodes.
$n$ exponent in the relation to compute the channel width as a function of the flow discharge.
$n_a$ parameter to compute the active layer thickness as a function of the $D_{s90}$.
$n_k$ parameter to compute the roughness height as a function of the $D_{s90}$.
$n_{\text{step}}$ number of calculations done for each value of flow discharge.
$N_{\text{disc}}$ number of discharge bins in the input hydrograph.
$p_i$ fraction of sediment of the bed load in the $i$th size range.
$q_{bi}$ grain size–specific bed load transport rate per unit channel width.
$q_{bT}$ total bed load transport rate per unit channel width.
$q_w$ water discharge per unit channel width.
$Q_w$ water discharge.
$Q_{w\text{ref}}$ reference discharge.
$R$ submerged specific gravity of the sediment.
$S$ bed slope.
$t$ time.
$u_*$ shear velocity.
$W_i^*$ grain size–specific bed load transport rate.
$x$ down-channel coordinate.
$\alpha_r$ coefficient in the Manning-Strickler resistance relation.
$\Delta_{tf}$ temporal step length in flood days.
$\Delta_{tw}$ duration of each discharge bin of the hydrograph.
$\eta$ bed elevation.
$\eta_d$ downstream bed elevation.
$\lambda_p$ bed porosity.
$\rho$ density of water.
$\rho_s$ density of sediment.
$\tau_{sg}^*$ Shields parameter computed as a function of the geometric mean diameter of the bed surface.
$\tau_{ssrg}^*$ reference or critical Shields parameter for the load relation of *Wilcock and Crowe* [2003].
$\phi_i$ nondimensional parameter to compute the grain size-specific bed load transport rate with the load relation of *Wilcock and Crowe* [2003].

[133] **Acknowledgments.** This paper represents a contribution of the National Center for Earth-surface Dynamics, a Science and Technology Center funded by the U.S. National Science Foundation (EAR-0203296). Special thanks are owed to Esther Eke for the discussions on mobile bed equilibrium and hydrograph boundary layer.

## References

Gaeuman, D. (2008a), Estimated fractional bedload inputs to the Trinity River from tributaries from Lewiston Dam to Trinity House Gulch, *Tech. Memo. TM-TRRP-2008-1*, Trinity River Restor. Program, Weaverville, Calif.

Gaeuman, D. (2008b), Recommended quantities and gradation for long-term coarse sediment augmentation downstream from Lewiston Dam, *Technical Memo. TM-TRRP-2008-2*, Trinity River Restor. Program, Weaverville, Calif.

Gaeuman, D., E. D. Andrews, A. Krause, and W. Smith (2009), Predicting fractional bed load transport rates: Application of the Wilcock-Crowe equations to a regulated gravel bed river, *Water Resour. Res.*, *45*, W06409, doi:10.1029/2008WR007320.

Graham Matthews and Associates (2001), Sediment source analysis for the Mainstem Trinity River, Trinity County, CA, report, 190 pp., TetraTech, Inc. Weaverville, Calif.

Graham Matthews and Associates (2006), Upper Trinity River sediment source analysis, Trinity County Resour. Conserv. Dist., Weaverville, Calif.

Grant, G. E., J. C. Schmidt, and S. L. Lewis (2003), A geological framework for interpreting downstream effects of dams on rivers, in *A Peculiar River: Geology, Geomorphology, and Hydrology of the Deschutes River*, *Water Sci. Appl. Ser.*, vol. 7 edited by J. E. O'Connor and G. E. Grant, pp. 209–225, AGU, Washington, D. C.

Harvey, B., S. McBain, D. Reiser, L. Rempel, L. Sklar, and R. Lave (2005), Key Uncertainties in Gravel Augmentation: Geomorphological and Biological Research Needs for Effective River Restoration, 99 pp., CALFED Science and Ecosystem Restoration Programs, Sacramento, Calif.

Hassan, M. A., E. Roey, and G. Parker (2006), Experiments on the effect of hydrograph characteristics on vertical grain sorting in gravel bed rivers, *Water Resour. Res.*, *42*, W09408, doi:10.1029/2005WR004707.

Hirano, M. (1971), On riverbed variation with armoring (in Japanese), *Proc. Jpn. Soc. Civ. Eng.*, *195*, 55–65.

Hoey, T. B., and R. I. Ferguson (1994), Numerical simulation of downstream fining by selective transport in gravel bed rivers: Model development and illustration, *Water Resour. Res.*, *30*, 2251–2260.

Knott, J. M. (1974), Sediment discharge in the Trinity River basin California, *U.S. Geol. Surv. Water Resour. Invest. Rep.*, *49-73*.

Kondolf, G. M. (2000), Assessing salmonid spawning gravel quality, *Trans. Am. Fish. Soc.*, *129*, 262–281.

Kondolf, G. M., and J. T. Minear (2004), Coarse sediment augmentation on the Trinity River below Lewiston Dam: Geomorphic perspectives and review of past projects, report, Trinity River Restor. Program, Weaverville, Calif.

Kondolf, G. M., and G. M. Wolman (1993), The sizes of salmonid spawning gravel, *Water Resour. Res.*, *29*(7), 2275–2285.

Lisle, T. E., and S. Hilton (1992), The volume of fine sediment in pools: An index of sediment supply in gravel-bed streams, *Water Resour. Bull.*, *28*(2), 371–383.

May, C. L., B. Pryor, T. E. Lisle, and M. Lang (2009), Coupling hydrodynamic modeling and empirical measures of bed mobility to predict the risk of scour and fill of salmon redds in a large regulated river, *Water Resour. Res.*, *45*, W05402, doi:10.1029/2007WR006498.

McBain, S., and B. Trush (1997), Thresholds for managing regulated river ecosystems, in *Proceedings of the Sixth Biennial Watershed Management Conference*, edited by S. Sommarstrom, *Water Resour. Cent. Rep. 92*, pp. 11–13, Univ. of Calif., Davis.

Moffett, J. W., and S. E. Smith (1950), Biological investigations of the fishery resources of Trinity River, California, *Spec. Sci. Rep. Fish. 12*, U.S. Dep. of the Inter. Fish and Wildl. Serv., Washington, D. C.

Nelson, R. W., J. R. Dwyer, and W. E. Greenberg (1987), Regulated flushing in a gravel-bed river for channel habitat maintenance: A Trinity River fisheries case study, *Environ. Manage*, *11*(4) 479–493.

Parker, G. (1991a), Selective sorting and abrasion of river gravel. I: Theory, *J. Hydraul. Eng.*, *117*(2), 131–149.

Parker, G. (1991b), Selective sorting and abrasion of river gravel. II: Applications, *J. Hydraul. Eng.*, *117*(2), 150–171.

Parker, G., and P. Klingeman (1982), On why gravel bed streams are paved, *Water Resour. Res.*, *18*(5), 1409–1423.

Parker, G., and C. M. Toro-Escobar (2002), Equal mobility of gravel in streams: The remains of the day, *Water Resour. Res.*, *38*(11), 1264, doi:10.1029/2001WR000669.

Parker, G., and P. R. Wilcock (1993), Sediment feed and recirculating flumes: A fundamental difference, *J. Hydraul. Eng.*, *119*(11), 1192–1204.

Parker, G., S. Dhamotharan, and S. Stefan (1982), Model experiments on mobile paved gravel bed streams, *Water Resour. Res.*, *18*(5), 1395–1408.

Parker, G., M. Hassan, and P. R. Wilcock (2008), Adjustment of the bed surface size distribution of gravel-bed rivers in response to cycled hydrographs, in *Gravel-Bed Rivers VI: From Process Understanding to River Restoration*, edited by H. Habersack, H. Piégay, and M. Rinaldi, pp. 241–285, Elsevier, New York.

Pitlick, J., and P. R. Wilcock (2001), Relations between streamflow, sediment transport and aquatic habitat in regulated rivers, in *Geomorphic Processes and Riverine Habitat*, *Water Sci. Appl. Ser.*, vol. 4, pp. 185–198, AGU, Washington, D. C.

Toro-Escobar, C. M., G. Parker, and C. Paola (1996), Transfer function for the deposition of poorly sorted gravel in response to streambed aggradation, *J. Hydraul. Res.*, *34*(1), 35–53.

Trso, M. (2004), Evaluation of Grass Valley Creek watershed restoration activities, report Trinity River Restor. Program, Weaverville, Calif.

U.S. Fish and Wildlife Service and Hoopa Valley Tribe (1999), Trinity River flow evaluation, final report, 1999, U. S. Dep. of the Inter., Washington, D. C.

Viparelli, E., O. Sequeiros, A. Cantelli, P. R. Wilcock, and G. Parker (2010), Modeling of river morphodynamics with creation/consumption of grain size stratigraphy. Part 2: Numerical model, *J. Hydraul. Res.*, *48*(6), 727–741.

Wilcock, P. R., and J. C. Crowe (2003), Surface-based transport model for mixed-size sediment, *J. Hydraul. Eng.*, *129*(2), 120–128.

Wilcock, P. R., G. M. Kondolf, W. V. G. Matthews, and A. F. Barta (1996), Specification of sediment maintenance flows for a large gravel-bed river, *Water Resour. Res.*, *32*(9), 2911–2921.

Williams, G. P., and M. G. Wolman (1984), Downstream effects of dams on alluvial rivers, *U.S. Geol. Surv. Prof. Pap.*, *1286*.

Wong, M., and G. Parker (2006), One-dimensional modeling of bed evolution in a gravel bed river subject to a cycled flood hydrograph, *J. Geophys. Res.*, *111*, F03018, doi:10.1029/2006JF000478.

D. Gaeuman, Trinity River Restoration Program, PO Box 1300, 1313 S. Main St., Weaverville, CA 96093, USA.

G. Parker and E. Viparelli, Department of Civil and Environmental Engineering, University of Illinois at Urbana-Champaign, Urbana, IL 61801, USA. (eviparel@illinois.edu)

P. Wilcock, Department of Geography and Environmental Engineering, Johns Hopkins University, 3400 N. Charles St., Ames Hall 313, Baltimore, MD 21218, USA.